Finite element analysis for a deep excavation in soft clay supported by lime-cement columns

Computers and Geotechnics 162 (2023) 105687

Contents lists available at ScienceDirect

Computers and Geotechnics

journal homepage: www.elsevier.com/locate/compgeo

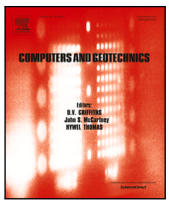

Research paper

Finite element analysis for a deep excavation in soft clay supported by lime-cement columns

Sinem Bozkurt *, Ayman Abed, Minna Karstunen

Chalmers University of Technology, Department of Architecture and Civil Engineering, Gothenburg, SE-412 96, Sweden

ARTICLE INFO

Keywords:
Deep excavation
Deep mixing
Lime-cement columns
Soft soil
Constitutive models

ABSTRACT

The aim of the paper is to simulate the response of a deep excavation supported by sheet pile walls and lime-cement columns. The application of the deep mixing technique using lime-cement products in deep excavations changes the initial state of the natural soil and creates substantial displacements associated with the installation effects. In this paper, the influence of lime-cement stabilisation was investigated using the finite element method for an instrumented braced excavation. The 2D finite element analyses were performed with advanced constitutive models for both natural clay and stabilised soil, exploiting the laboratory test made on both field mixed and laboratory mixed stabilised clay samples. The numerical results show that taking account of installation effects provides realistic predictions of deformation, excess pore water pressure evolution, as well as the structural forces in the struts.

1. Introduction

Ground improvement with deep mixing methods using lime and/or cement as binders has been used extensively since the late 1960s. The advantages of the deep mixing method over other methods, such as bored or displacement piling methods include lower construction cost, reduced cumulative energy consumption (Zöhrer and Stelte, 2010), and the successful execution rate on various soil types for limiting settlements and vibrations.

In Sweden, field applications started with the use of the dry soil mixing (DSM) method. DSM is often called as the 'Nordic Method' since it was widely established in Nordic countries by the end of the 1980s (Holm, 2003). The method uses dry cementitious binders that undergo hydration with the water in the natural soil, which is abundant in sensitive clays with natural water content exceeding the liquid limit. Field applications are often executed using a combination of quicklime (unslaked lime) and Portland cement as the main mixing agents. For the details of the current design methodologies in Sweden, the reader is referred to Larsson (2003, 2017).

While under embankment loading individual columns are most often preferred (e.g. Kawasaki, 1981; Kitazume and Maruyama, 2006; Krenn and Karstunen, 2008; Vogler, 2009), deep mixing with overlapping columns is commonly used among other ground improvement methods for braced excavations in soft clays (i.e. Tanaka, 1993; O'Rourke and O'Donnell, 1997; Ou et al., 2008; Ignat et al., 2016, 2020) and slopes (i.e. Jamsawang et al., 2015, 2016; Marte et al., 2017). The overlapping columns reinforce the excavation bottom in order to reduce vertical and lateral displacements, and thus improve the soil against basal heave failure.

During the mixing process, typically, the strength and the stiffness of soil increase (Holm, 2003). Field performance of the deep mixed columns in braced excavations is influenced by many factors. These include properties of the in situ soil, mixing procedure, and installation effects during and after the mixing. Soil disturbance due to high air-pressured injection of admixtures using rotating blades, chemical reactions, and the interactions between the binders and the soil (e.g., excess pore pressure generation, soil fracturing, thixotropy, consolidation, cementation, temperature changes etc.) are the main contributors to the installation effects. Although the primary governing mechanism affecting the stress–strain response of stabilised soil is unloading caused by the excavation, the observed deformations prior to the actual excavation necessitate the consideration of the installation effects. Lateral wall deformations and heave behind the wall can be observed in the case where the soil stabilisation is applied after the sheet pile wall (SPW) construction (O'Rourke and O'Donnell, 1997). These deformations caused by the installation of deep mixed columns are akin to those of pile driving (Randolph et al., 2015). Installation-induced deformations have been linked to soil disturbance and thixotropy (Broms, 1999; O'Rourke and O'Donnell, 1997; Shen et al., 2003a,b). Although the surrounding soil regains its strength following the curing period (Shen et al., 2003a,b), the deformations caused by the loss of soil resistance, generated by the use of high-air

* Corresponding author.
E-mail address: sinem.bozkurt@chalmers.se (S. Bozkurt).

https://doi.org/10.1016/j.compgeo.2023.105687
Received 5 May 2023; Received in revised form 7 July 2023; Accepted 19 July 2023
Available online 2 August 2023

pressure during the early stages of the mixing process, are essential for a realistic estimation of stress–strain response of braced excavations. The complex application procedure of DSM leads to serious challenges associated with the quantitative evaluation of the installation effects.

Conventionally in deep mixing design, due to the scarcity of high-quality laboratory and field testing data, linear elastic or liner elastic-perfectly plastic Mohr–Coulomb soil models are used (e.g. O'Rourke and O'Donnell, 1997; Baker et al., 2005; Consoli et al., 2014). Moreover, current design guidelines (i.e. Stab, 2002; Bruce et al., 2013; CEN, 2005; Trafikverket, 2014) rely heavily on unconfined compressive strength (UCS, q_u) measured from uniaxial compression tests (UCT), and empirical relationships between q_u and the stiffness. Yet, in problems such as braced excavations supported by overlapping DSM columns, the response is dictated by the stiffness.

This study investigates the stress–strain response of a deep excavation supported by lime-cement columns in the passive side, taking into account the installation effects. A fully coupled 2D FE analysis was performed using advanced nonlinear constitutive soil models for both the natural and the stabilised clay. The model parameters are based on a series of experimental data. The laboratory testing data included anisotropically consolidated undrained triaxial compression and extension tests (CAUC/E), incrementally loaded oedometer (IL) tests, and constant rate of strain (CRS) tests that were performed on the natural clay, as well as both field-mixed and laboratory-mixed samples.

The calibration of the model parameters was carried out using the SoilTest facility in PLAXIS2D FE code (PLAXIS Material Model, 2021). The calibrated parameters were then used in modelling a case history of an 11 m-braced excavation supported by lime-cement columns in Gothenburg, Sweden. The deformations resulting from the installation effects of lime-cement columns were back-calculated based on inclinometer measurements and incorporated in the analysis by the use of prescribed volumetric strains. The 2D FE results were compared to the high-quality field monitoring data that came from inclinometers, pore pressure stations, and strain gauges installed on the struts. The following section gives a background on excavations in soft clays and modelling considerations.

2. Theoretical framework

Long-term deformation calculations of deep excavations stabilised by lime-cement columns are associated with difficulties in achieving reliable predictions of deformation, pore pressure distribution and structural forces, in particular when dealing with sensitive soft clays. The mechanical response of the natural clay is described by the adopted constitutive model, which in the case of soft natural clays should be able to capture the effect of typical features, such as fabric anisotropy, bonding, and strain-rate dependency.

Natural clay exhibits anisotropy due to stress history and the deposition process (Graham and Houlsby, 1983; Karstunen and Koskinen, 2008; Wheeler et al., 2003). Ignoring the effect of anisotropy and evolution of anisotropy results in underestimation of deformation of the soft clay (Karstunen et al., 2005; Yin et al., 2011; Kavvadas and Amorosi, 2000). Furthermore, the use of isotropic constitutive models leads to inaccurate prediction of the mobilised undrained shear strength (Pande and Sharma, 1983; Leoni et al., 2008).

The failure mechanism of the excavations in soft clays is affected by anisotropy due to the significant rotation of principal stresses (Clough et al., 1981; Finno and Nerby, 1989). Below the bottom of the excavation, the reorientation of principle stresses varies between 0°–90° (Clough et al., 1981). The stress reorientation leads to changes in the mobilised shear strength, and necessities the use of advanced soil models that incorporate kinematic hardening (e.g. SCLAY1S (Wheeler et al., 2003), Creep SCLAY1S (Sivasithamparam et al., 2015; Gras et al., 2018), MSS (Kavvadas and Amorosi, 2000)).

Another major challenge in predicting long-term deformation of braced excavations is due to the compressibility of the soft clays, which is dependent on both time and effective stress level (Leroueil et al., 1985). Several studies have been conducted to include the rate dependency within the framework of critical state models (Leoni et al., 2008; Grimstad et al., 2010; Yin et al., 2011; Yin and Graham, 2011; Olsson, 2013; Sivasithamparam et al., 2013, 2015; Yang et al., 2015). The Creep-SClay1S model adopted in this study is not only able to capture the rate dependency, but also anisotropy and destructuration (changes in fabric and interparticle bonding) as necessary for sensitive clays.

Stress–strain response of deep excavations improved with DSM is influenced by the properties of both the natural and stabilised clay. For instance, there is a wide variety of soft clays only in Sweden, with vastly different compressibilities and overconsolidation ratios resulting from dissimilar deposition history, varied sensitivity, mineralogy, water and fines content, and the presence of organic materials. Moreover, the rheological properties of the stabilised clays are also affected by various factors such as characteristics of the binder (type, quality, and quantity), geotechnical conditions, the properties of the natural clay, the mixing process (blade rotation number, configuration) and the curing conditions (temperature, time, stresses) (Holm, 2003). Therefore, the design of soil improvement for deep excavations requires a comprehensive site and laboratory investigation to designate representative geotechnical parameters of both in situ clay and the soil mixture.

Deep soil mixing changes the initial stress distribution in the soft clays leading to considerable deformations prior to excavation, as seen in O'Rourke and O'Donnell (1997) and in this study. Thus, realistic estimation of the deformations require some consideration of the installation effects.

The predictions of the ground movements resulting from excavations constructed in soft clay necessitate the consideration of the most unfavourable condition. The critical condition for excavations in normally consolidated saturated clays is the long-term behaviour, due to the dissipation of the negative excess pore pressures (Lambe and Whitman, 1969; Eigenbrod, 1975). The gradual decrease in the negative pore pressures at the bottom of the excavation pit leads to a decrease in the effective stresses and, as a consequence, a reduction in the undrained shear strength. Therefore, the total pore pressures measured immediately after the excavation at the passive zone would be lower than the ultimate values (Ghadrdan et al., 2020). To capture these processes, it was necessary for this study to carry out a fully coupled hydro-mechanical analysis for the long-term conditions. In fact, both short-term and long-term conditions can be evaluated based on coupled analyses that allow for a realistic calculation of time-dependent transient flow simultaneously with the mechanical response of the in situ and the stabilised clay during the progression of the excavation.

3. Site location and geotechnical conditions

West Link project is a railway project in Gothenburg consisting of a construction of an eight-kilometre-long double-track railway, including a six-kilometre railway tunnel, underneath the city (Fig. 1). E02 Central Station is a major part of this project, located in the centre of Gothenburg. The research focuses on the investigation of approximately a 40-m long temporary excavation. The temporary excavation was instrumented and monitored for a period of 8 months before the installation of the final concrete tunnel.

The braced excavation was supported by sheet pile walls (SPWs), lime-cement columns, and two levels of struts. The SPWs, as the primary structural support, had the profile AZ-38-700N, while the steel struts with circular cross-sections were connected to the sheet piles via waler beams (HEB500-800).

The passive side of the excavation was supported by double overlapped columns in a rectangular grid of interlocking pattern with 2.5 m spacing. The DSM columns with a diameter of 70 cm were installed with an overlap of 20 cm. In order to accomplish an economic design, different lime-cement binder ratios were utilised below (80 kg/m^3) and

Fig. 1. E02 West Link project Central Station district. 57° 71′ 30" N, 11° 98′ 22" E, Elevation 1.85 m. GoogleEarthh V 9.148.0.0. https://earth.google.com/web/ [Accessed April 19, 2023]. Project location: https://upload.wikimedia/V\"astl\"anken.org.

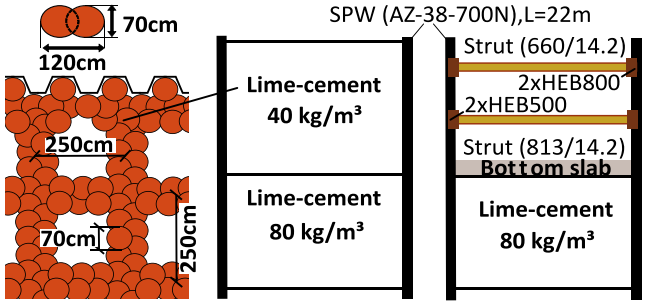

Fig. 2. Plan view and cross-section of E02 Central station deep excavation of West Link project.

above (40 kg/m^3) the final excavation level. The plan view and the location of the studied cross-section of the braced support system are illustrated in Fig. 2.

Field measurement devices, including inclinometers, pore pressure probes, prisms recording surface displacements, and strain gauges assembled on the struts were installed in specific coordinates to monitor the performance of the braced excavation as part of the Observational Method (Peck, 1969). The location of the field monitoring devices is presented in Fig. 3.

A comprehensive geotechnical site investigation was conducted to characterise the properties of the soft natural clay and the lime-cement columns in the Central Station area of Gothenburg by the Swedish Transport Administration (2018). The soil deposit consists mainly of soft, high-plastic glacial, and post-glacial clay to a depth of 55–75 m (Swedish Transport Administration, 2019). The soft clays were deposited in glaciomarine environment during the late Weichselian times due to the deglaciation in the Gothenburg area (Stevens and Bayard, 1994). Later, the depositional environment evolved by isostatic uplift and climate change (Stevens et al., 1991).

The soil stratigraphy consists of a 2 to 5-m thick layer of fill underlain by a deep clay deposit. In the central area of Gothenburg, there is a significant amount of fill moved during the 19th century which is the main contributor to the ongoing creep settlements (Tornborg et al., 2021). The groundwater level is located at a depth of 2–3 m with some seasonal fluctuations.

Constant rate of strain (CRS) and incrementally loaded (IL) oedometer test data indicated that the layers are typically normally consolidated to slightly overconsolidated with an overconsolidation ratio (OCR) in the range of 1.00 to 1.50. Soil deposit was characterised as normally consolidated after a depth of 30 m. Low OCR measurements in the deep clay layers could be resulting from sample disturbance. Fig. 4 shows the index properties. The unit weight varies between 15.5 and 16.5 kN/m^3. The deposit has sensitivity (S_t) that varies in the range of 10–30 (classified as medium sensitive according to Rankka et al. (2004)).

Table 1
Creep SCLAY1S model parameters.

Type	*Parameter*	*Definition*
Stiffness	κ^*	Modified swelling index
	λ_i^*	Modified intrinsic compression index
	ν'	Poisson'sratio
Strength	M_c	Critical state stress ratio in compression
	M_e	Critical state stress ratio in extension
Anisotropy	ω	Absolute effectiveness of rotational hardening
	ω_d	Relative effectiveness of rotational hardening
Destructuration	a	Absolute rate due to volumetric strain
	b	Relative rate due to deviator strain
Viscous	μ_i^*	Modified intrinsic creep index
	τ	Reference time (days)
Initialisation	e_0	Initial void ratio
	σ_p'	Preconsolidation pressure (kPa)
	K_0	Coefficient of earth pressure at rest
	α_0	Initial anisotropy
	χ_0	Initial amount of bonding

4. Numerical model of the deep excavation in the Central Station

This section presents the finite element model, including the employed constitutive models, calibration of the parameters, the finite element mesh, and boundary conditions.

4.1. Constitutive models

Creep-SCLAY1S model for soft clay

The Creep-SCLAY1S (Sivasithamparam et al., 2015; Gras et al., 2018) is the rate dependent successor of the SCLAY1S model (Wheeler et al., 2003). Creep-SCLAY1S accounts thus for anisotropy, degradation of bonding, and rate dependency of soft clay. Creep-SCLAY1S comprises three hardening laws that control the changes in the Normal Compression Surface in terms of size, rotation, and progressive loss of bonding with (irrecoverable) volumetric (ε_v^c) and deviatoric (ε_d^c) creep straining. A full description of the model can be found in Appendix A.

The model has no pure elastic range. The rate-dependency can be derived directly from experimental data through the concept of a visco-plastic multiplier based on Grimstad et al. (2010). Some of the advantages of using the model are the prediction of dilation on the 'dry' side of the critical state line (Sivasithamparam et al., 2013) and a realistic calculation of K_0^{NC}, the coefficient of earth pressure in the normally consolidated region.

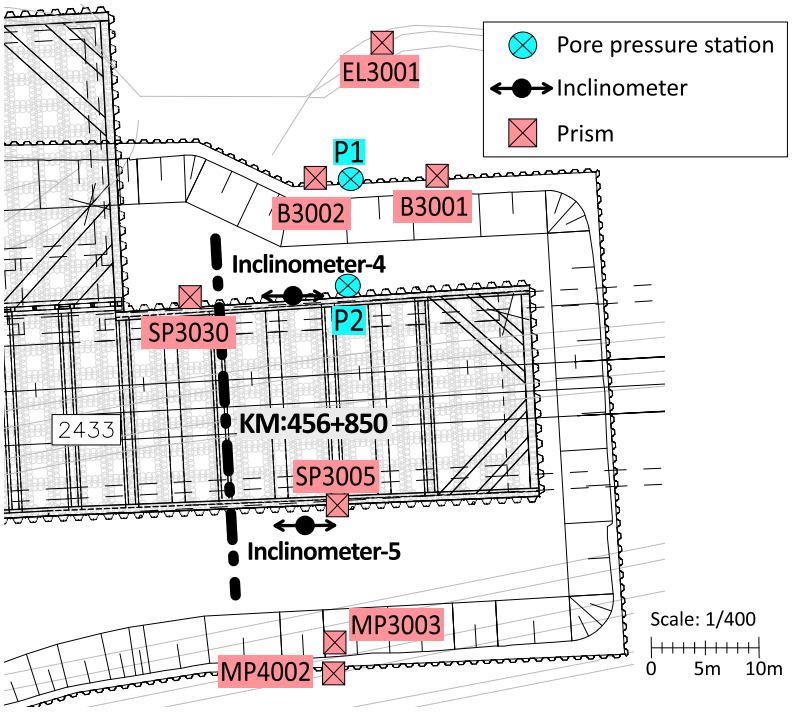

Fig. 3. Location of the inclinometers in the field.

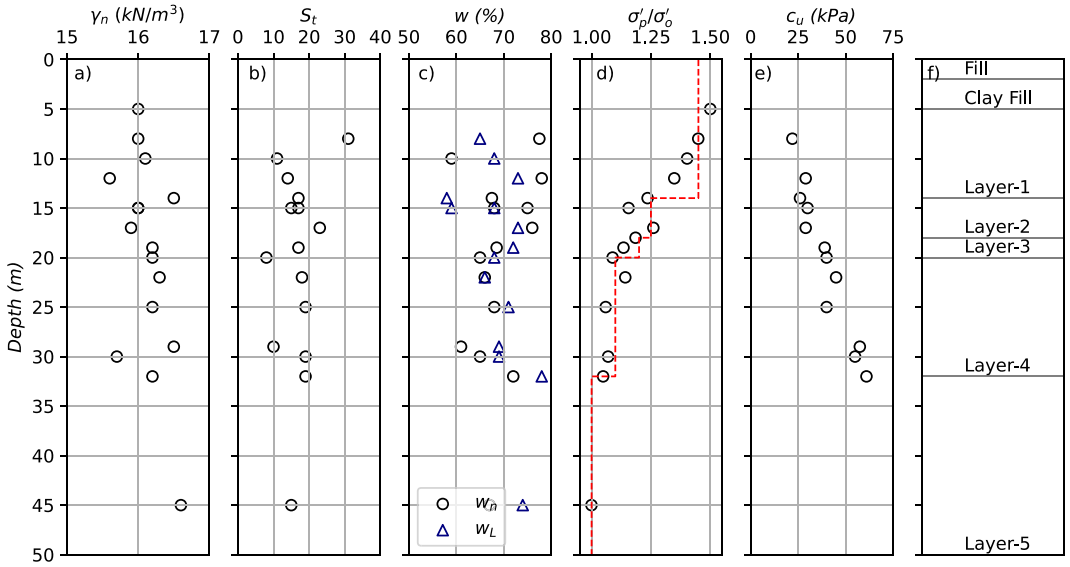

Fig. 4. Index properties of Gothenburg clay at the Central Station. (a) Natural unit weight, (b) sensitivity, (c) natural water content and liquid limit, (d) the ratio of preconsolidation stress to vertical effective stress (OCR), (e) undrained shear strength (f) assumed layering.

The model parameters can be estimated using routine laboratory testing: anisotropically consolidated (undrained and drained) triaxial compression (CAUC/CADE) and extension (CAUC/CAUE) tests, as well as incrementally loaded oedometer (IL) tests. The calibration of the soil parameters has been described in detail in Gras et al. (2017, 2018). Creep-SCLAY1S model parameters are presented in Table 1 and more details can be found in Appendix A.

MNhard for lime-cement columns

The MNhard (Matsuoka–Nakai Hardening) material model (Benz et al., 2008) has a similar formulation to the well-known Hardening Soil model (HS) (Schanz, 1998; Schanz et al., 1999) in terms of shear hardening, however, it does not consider any volumetric hardening. Another difference is that the MNhard model adopts the Matsuoka–Nakai (MN) (Matsuoka and Nakai, 1974, 1982) as the failure criterion instead of Mohr–Coulomb. Shear hardening during triaxial primary loading is defined through the following yield function (Eq. (1)).

$$f_s = \frac{3}{4}\frac{q_a}{E'_{50}}\frac{q}{q_a - q} - \frac{3}{2}\frac{2q}{E'_{ur}} - \gamma^{ps} \text{ and } R_f = \frac{q_f}{q_a} < 1.0 \quad (1)$$

where E'_{50} and E'_{ur} are the secant and unloading–reloading stiffness respectively, γ^{ps} is the material variable describing the accumulated deviatoric plastic shear strain ($\gamma^{ps} = 3/2\varepsilon_1^p$) (Benz et al., 2008). Yield locus expands with the plastic shear strains due to deviatoric loading ($q = \sigma'_1 - \sigma'_3$, $\sigma'_1 \geq \sigma'_2 = \sigma'_3$) until the MN failure condition is reached. The model adopts effective minor stress-dependent stiffness by Eq. (2).

Table 2
Creep-SCLAY1S model parameters for Gothenburg clay at Central Station.

Layer	λ_i^*	κ^*	ν'	M_c	M_e	ω	ω_d	a	b	μ_i^*	τ (day)
Layer-1 and Clay fill	0.085	0.006	0.20	1.45	0.97	20	0.98	12	0.2	0.006	1
Layer-2	0.080	0.008	0.20	1.18	1.15	35	0.74	12	0.2	0.006	1
Layer-3	0.085	0.007	0.20	1.10	0.99	50	0.64	12	0.4	0.006	1
Layer-4	0.080	0.005	0.20	1.12	0.99	50	0.66	12	0.2	0.006	1
Layer-5	0.085	0.008	0.20	1.10	1.20	50	0.70	12	0.2	0.006	1

Table 3
State parameters and additional model parameters for the clay layers at Central Station.

Layer	OCR	e_0	α_0	χ_0	K_0	c_k[b]	$k_h = k_v (m/day)$
Clay fill	1.45	1.91	0.56	6	0.52	0.95	0.56×10^{-4}
Layer-1	1.45	2.24	0.56	6	0.52	0.44	1.30×10^{-4}
Layer-2	1.25	1.97	0.45	6	0.59	0.24	0.63×10^{-4}
Layer-3	1.20	1.90[a]	0.42	6	0.58	0.27[a]	0.75×10^{-4}[a]
Layer-4	1.10	1.83	0.43	6	0.55	0.30	0.86×10^{-4}
Layer-5	1.00	1.69	0.44	6	0.52	0.29	0.52×10^{-4}

[a]The average permeability values of the lower and upper clay layers were used. The results of the CRS tests performed on soft clay samples were given in Appendix C.
[b]The permeability change index, $c_k = \frac{e_0 - e}{\log(k_0/k)}$, where k_0 is the permeability corresponding to e_0 and k denotes the hydraulic conductivity at a void ratio, e (Tavenas et al., 1983).

$$E'_{50} = E'^{\,ref}_{50} \left(\frac{\sigma'_3 + c' \cot \phi'}{\sigma'^{ref} + c' \cot \phi'} \right)^m \tag{2}$$

where $E'^{\,ref}_{50}$ is the reference secant modulus corresponding to reference stress σ'^{ref}, σ'_3 is the confining stress, and the exponent of m defines the shape of the yield loci, reflecting the amount of stress dependency of the stiffness (Vermeer and Brinkgreve, 1998). For granular materials, the value ranges between 0.5–1.0 (Benz, 2007). Un-/reloading stress condition is assumed to be purely elastic (nonlinear). Similar to the secant modulus, the tangent unloading-reloading modulus is defined by Eq. (3).

$$E'_{ur} = E'^{\,ref}_{ur} \left(\frac{\sigma'_3 + c' \cot \phi'}{\sigma'^{ref} + c' \cot \phi'} \right)^m \tag{3}$$

The MN failure criterion employs the concept of the average of mobilised planes (SPM, 'spatially mobilised plane') in three-dimensional stress space where the maximum ratio of the shear, τ_{SMP} and normal stresses, σ'_{SMP} occurs. Once failure condition is satisfied, τ_{SMP}/σ'_{SMP} takes the limiting value (Eq. (4)).

$$f_{MN} = \frac{I_1 I_2}{I_3} - c \quad with\ c = \frac{9 - \sin \phi'^{\,2}_m}{-1 + \sin \phi'^{\,2}_m} \tag{4}$$

where I_1, I_2, I_3 are the first, second, and third effective stress invariants, respectively. Shear modulus during unloading-reloading (G_{ur}) can be defined by the assumption of purely (nonlinear) elastic behaviour (Eq. (5)).

$$G_{ur} = \frac{1}{2(1 + \nu_{ur})} E'_{ur} \tag{5}$$

where ν_{ur} is Poisson's ratio for unloading-reloading.

4.2. Parameters of the numerical model

Soft Clay

The model parameters of Creep-SCLAY1S were obtained from laboratory tests (CADC/E and CAUC/E, CRS and IL) performed on undisturbed natural clay samples. The parameters were first estimated using the method described in Gras et al. (2017, 2018) and then calibrated via simulations. The calibrated model parameters are presented in Tables 2 and 3.

The comparison of the laboratory test simulations with the original IL test data is presented in Fig. 5 at the depths of 8, 12, 15, 17, 19, 20, 22, 25, and 32 m. The simulations were also performed for drained and undrained triaxial tests at different depths along the soil profile. These results, shown in Fig. 6, demonstrate that Creep-SCLAY1S model is able to replicate the soft clay response during CAUC/E and CADC/E tests on Gothenburg clay.

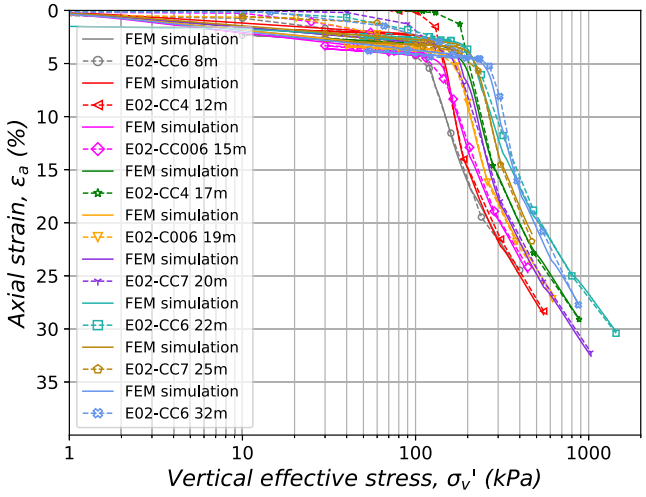

Fig. 5. Calibration of IL tests using the laboratory test simulations on Gothenburg clay samples.

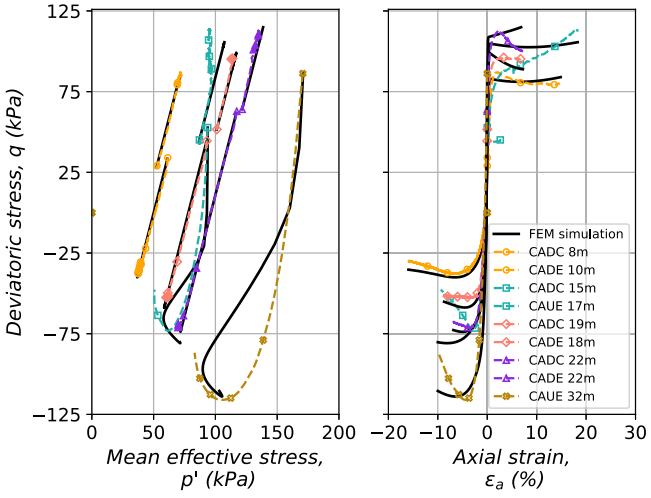

Fig. 6. Calibration of CADC/E and CAUC/E tests using the laboratory simulation on Gothenburg clay samples.

Lime-cement columns

Lime-cement (LC) column installation using the DSM method includes several processes that cause alternation in soil initial conditions: (1) soil disturbance by the mixing procedure (the application of compressed air, admixture injection, blade rotation), (2) soil fracturing and thixotropy resulting from soil disturbance, (3) ongoing chemical reactions within stabilised clay resulting in temperature increase, (4) ion

exchange between the surrounding soil and the admixtures and (5) consolidation (dissipation of excess pore air and water pressures) (Holm, 2003; Shen et al., 2003a,b).

The observed deformations, prior to excavation, due to mixing can be expansive or contractive. Usually, LC treatment of clay requires compaction to reduce the ratio of air voids to no more than 5% (Oates, 2008). In Sweden, DSM is done using compressed air, and no separate compaction is applied, except for the compaction arising from the mixing tool itself (Larsson, 2003). Therefore, the large amounts of air injected into the soil tend to cause an expansion within the stabilised area. Following the mixing, the stabilised clay undergoes consolidation without any mechanical compaction.

The expansion ratio of the deep-mixed columns can be measured based on experimental data for wet-mix columns. Shen et al. (2003a) introduced an empirical equation that considers the volume of injected slurry, the radius of the columns after hardening, the nominal radius of the mixing blade, and the volume factor. The expansion ratio of the column radius to the mixing blade radius was assumed to be proportional to the ratio of the injected slurry volume to the nominal column volume calculated by the blade radius. The equation accounts for the volume loss of slurry due to soil swelling and penetration into surrounding soil through fractures by using a volume factor ranging from 47%–70%, which represents the volume change caused by these effects. However, difficulties in measuring the volume change of highly inhomogeneous columns, and incorporating stress dependency of the hardened column volume into Shen et al. (2003a)'s equation along the improved zone necessitate further investigation. The volume changes resulting from the chemical processes (e.g., hydration, pozzolanic reactions, flocculation–coagulation, cementation, and drying) are highly dependent on the amount of used *lime* and *high/low alkali cement* (Taylor et al., 1997; Lorenzo and Bergado, 2006).

Contraction-induced deformations have been linked to soil disturbance, thixotropy and consolidation (Broms, 1999; O'Rourke and O'Donnell, 1997; Shen et al., 2003a,b). The loss of soil resistance, however, may be regained after a short curing period due to thixotropic recovery (Shen et al., 2003a). After the high air pressure application is stopped, both excess pore air and water pressure generated in the soil start to dissipate. Thus, consolidation appears to be related to the contraction behaviour of the excavation pits stabilised with LC columns.

In the case of the presence of field measurements, the resulting strains arising from the installation effects can be evaluated simultaneously with the excavation stages (Finno and Nerby, 1989; O'Rourke and O'Donnell, 1997).

- *Laboratory tests on samples from Centralen*

To investigate the engineering properties of stabilised clay at Centralen, CAUE and IL tests were performed on both soil-mixed and laboratory-mixed samples. Throughout the preparation of laboratory-mixed samples and in the field applications, different lime-cement ratios ranging between 40–150 kg cement/m^3 were utilised (Table 4). The authors of this paper were not involved in planning the test programme and testing.

CAUE tests

During undrained triaxial tests, excess pore water pressure development within the stabilised clay samples is highly dependent on initial effective stresses, stress history, mineralogy and external loading conditions. Change in the pore water pressure in axial symmetry conditions can be simply defined by Skempton pore pressure parameter, B and parameter A using the change in major and minor stresses Eq. (6).

$$\Delta u = B\,[\Delta\sigma_3 + A\,(\Delta\sigma_1 - \Delta\sigma_3)] \tag{6}$$

Sampling, even for the perfect sampling conditions, generates suction within the sample owing to the removal of overburden. This process allows air to enter the pore spaces and reduced saturation in particular for coarse-grained materials such as silt and sand (Sanlon et al., 2021). In the case of full saturation, especially for normally consolidated soft clay with high saturation degree due below the groundwater level, B-value would be measured close to 1. However, B-value at 99.9% saturation could be as low as 0.51 for stiff (clays-sands) and 0.10 for very stiff soils (very high consolidated pressures) (Black and Lee, 1973). LC column behaviour is considered partially saturated (Broms, 2004). When performing undrained triaxial tests, 100% saturation may not be possible if the initial degree of saturation or the application of back pressure is low for partially saturated soils (Black and Lee, 1973). This phenomenon can be attributed to the existence of undissolved pore air in the surrounding pore water, which basically results in a diffusion problem related to the required time to compress the air out by applying back pressure (Black and Lee, 1973).

The application of back pressure to obtain full saturation is dependent on the degree of initial saturation of the soil sample, and it is almost impossible for stiff or very stiff soils. Ignat et al. (2019) performed several undrained and drained triaxial laboratory tests with the application of different back pressures on soft clay samples mixed with lime-cement products. These results suggest that full saturation required a back pressure of 400 kPa. The use of low back pressures resulted in partially saturated samples with low B-values, especially at low confining stress levels. Similarly, Åhnberg (2006) suggests using a back pressure of at least 400 kPa for stabilised clay samples to ensure entrapped air dissolution in pore water during the consolidation stage. The stabilised clay with LC may be classified as stiff to very stiff.

In order to simulate the field conditions and stress-dependent strain behaviour, it is essential to consider the degree of saturation of the stabilised samples in terms of Skempton B parameter. The laboratory tests (Table 5) performed on both laboratory-mixed and field-mixed samples at Centralen were simulated considering partial saturation (Fig. 7). The CAUE test response could be replicated only through the inclusion of partial saturation with parameter B equals to 0.6. Skempton B parameter might result to different values for different binders, binder ratios and mixing techniques.

Given that the problem under analysis involves an unloading scenario, the shear modulus was calculated using undrained triaxial extension tests. Stress–strain relationship for the triaxial tests is presented in Fig. 8. Apparently linear elastic behaviour was found to be dominant at low strain levels up to 12%. The stabilised clay samples thus exhibit almost linear elastic behaviour when the stress state is inside the yield surface, which is not the case for naturally structured or reconstituted soils (Yapage and Liyanapathirana, 2019). In Fig. 8, the triaxial tests performed on laboratory mixed samples (NCC 30 and NCC 31) revealed varying deviatoric stress at failure due to differences in the sample homogeneity during laboratory mixing and the use of different back pressure. However, despite the varied homogeneity, similar stiffness can still be inferred.

Overall, the field and laboratory mixed samples yielded almost identical stiffness values. The resemblance of the stiffness can also be seen in Fig. 9. Although the lime-cement ratios differ, based on the similar stiffnesses in all CAUE tests, the shear stiffness was assumed to be the same within the whole stabilised zone. The model parameters used in the simulations of the stabilised clay are summarised in Table 6.

IL tests

Oedometer tests on stabilised samples indicated that the values of the apparent preconsolidation pressure vary significantly between the laboratory-mixed and field-mixed samples. The values of preconsolidation pressure are around 1300 kPa for the tests on the field-mixed samples, and 500 kPa for the laboratory-mixed samples (Fig. 9). The laboratory mixed samples were not subjected to a consolidation phase, and thus the initial effective stress state in the field was not replicated. There is, however, a very similar response beyond the apparent preconsolidation pressure in terms of the oedometric modulus.

Similar results have been reported by Åhnberg et al. (2001) who performed several IL tests, uniaxial compression tests (UCT) and triaxial tests on laboratory-mixed samples with the dry mixing method, and

Table 4
Testing programme for laboratory and field samples with lime and cement.

Sample number	Curing time (days)	LC content (kg/m^3)	Sample and test type
NCC31	28	110	CAUE
NCC30		110	(Laboratory mixed sample)
NCC14	[c]	80	IL (Laboratory mixed sample)
NCC21		≥150	
NCC29		≥150	
NCC36		≥150	
B3 14 m	21	80	CAUE
B3 16 m	42		(Field mixed sample)
168-1	[c]	50	IL (Field mixed sample)
168-2			
Pelare 810		80	

[c]The curing time data for these samples was not available.

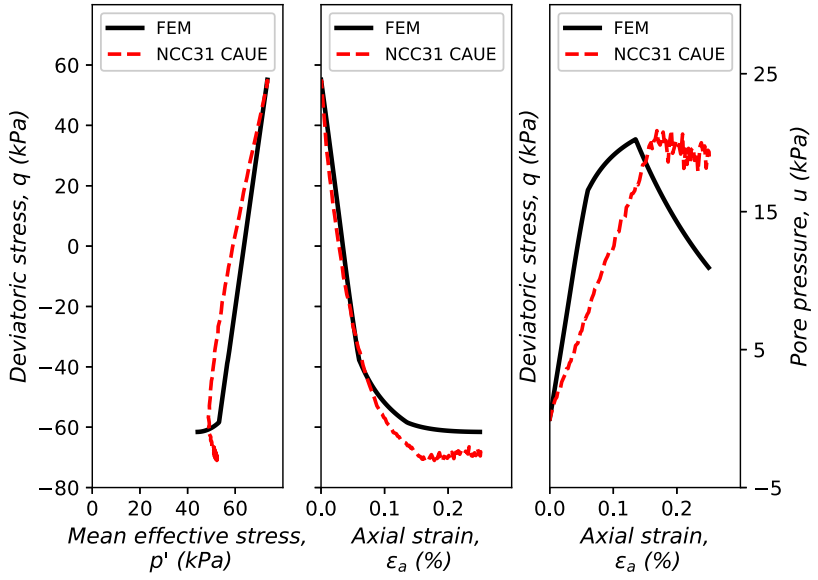

(a)

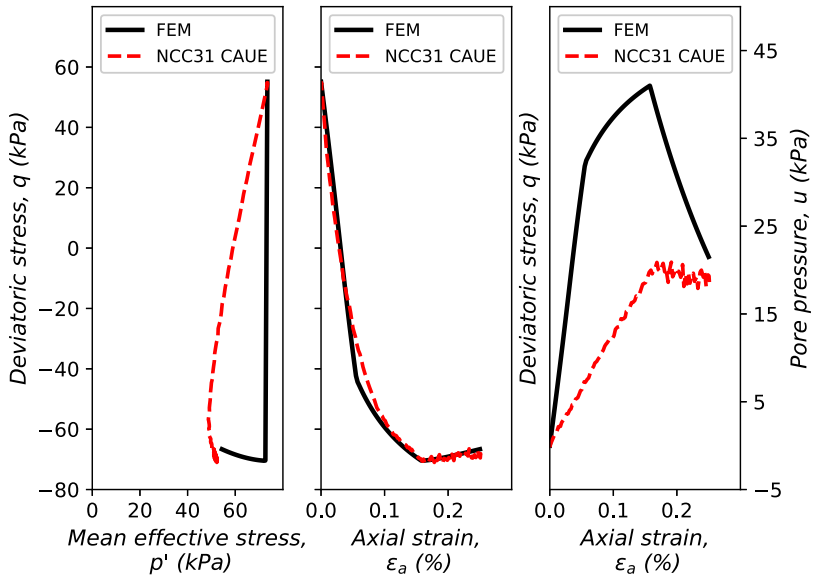

(b)

Fig. 7. MNhard soil model, the laboratory test simulation of CAUE test on a laboratory mixed sample for different Skempton B parameters: (a) B = 0.6, (b) B = 1.0.

Table 5
Failure stress and strain for laboratory and field mixed samples in the triaxial tests.

Sample number	$q_{failure}(kPa)$	$p'_{failure}(kPa)$	$\varepsilon_{failure}(\%)$	Back pressure (kPa)	Initial condition $\sigma'_{vertical}/\sigma'_{horizontal}$
NCC30	−50	51	0.04	135	110/55
NCC31	−71	52	0.17	300	
B3 14 m	−60	64	0.25	400	89/67
B3 16 m	−67	61	0.1	400	105/75

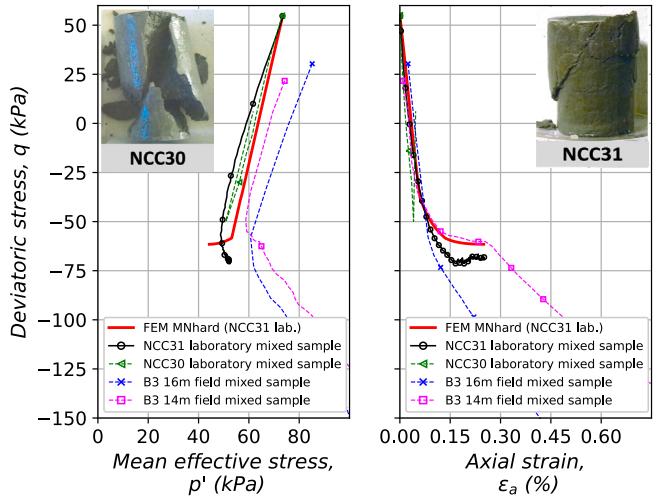

Fig. 8. CAUE tests and the laboratory test simulations on laboratory and field mixed samples.

Table 6
MNhard soil parameters for lime-cement columns using dry soil mixing method.

γ_n (kN/m^3)	G_{50}^{ref} (kPa)	G_{ur}^{ref} (kPa)	p^{ref} (kPa)	m	$\phi'(°)$	c' (kPa)	ν'	ν_{ur}
17	28000	75000	100	0.65	37	20	0.25	0.2

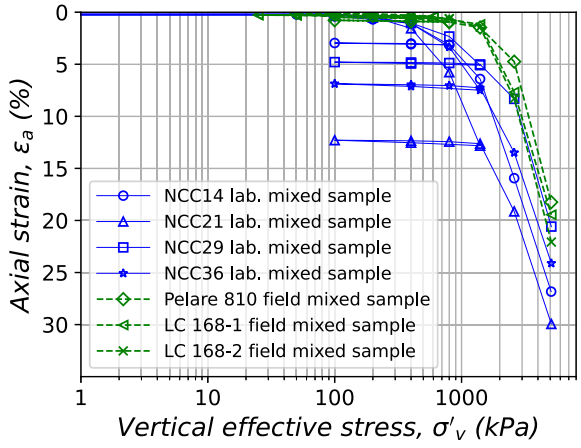

Fig. 9. IL tests on laboratory and field mixed samples.

investigated the initial load application during the hardening of the mixture. Given the very high values of the apparent preconsolidation pressures, it is highly unlikely that in practical applications any extra loading will lead to irrecoverable volumetric strains, thus the MNhard model was considered as a reasonable choice for modelling the stabilised clay. According to extensive laboratory tests, including IL and CAUC/E tests, general deformation and strength parameters of stabilised clay with LC agents are similar to those of partially saturated overconsolidated clays as stated in Broms (2004).

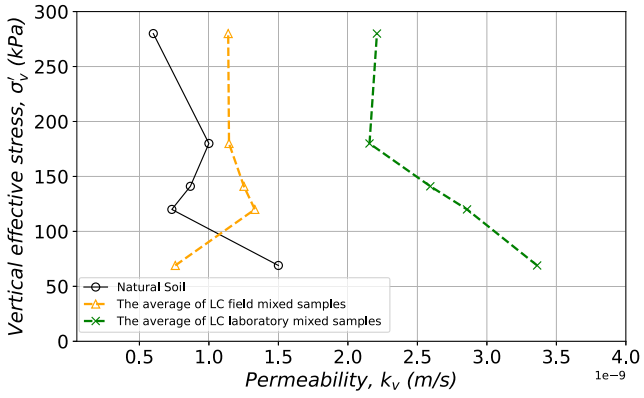

(a) Permeability of natural clay and LC column samples from IL tests.

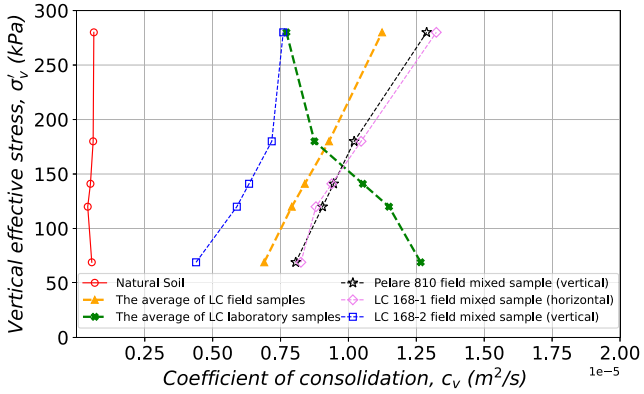

(b) Coefficient of consolidation of natural clay and LC column samples from IL tests.

Fig. 10. Hydraulic conductivity of the natural clay and the stabilised clay.

- *Hydraulic conductivity of the lime-cement columns*

The hydraulic conductivity (k) and the coefficient of consolidation (c_v) of the stabilised clay were compared with those of the natural clay (Fig. 10(a)). The samples taken from the field and mixed in the laboratory were subjected to IL tests (in Table 4). k values were found approximately equivalent to the values of the natural clay (Fig. 10(a)). Field-mixed samples taken from vertically and horizontally cut columns gave results of the same order. Similarly, research conducted by Wang and Tanttu (2018) on stabilised Otaniemi clay using dry soil mixing, as well as investigations on stabilised marine clays using wet mixing by Locat et al. (1996), O'Rourke and O'Donnell (1997), Yamadera et al. (1998), Horpibulsuk et al. (2003), Chew et al. (2004), all observed comparable k values to the values of the in situ clay. The k values of the stabilised clay roughly rely on the water content of the soil mix (Åhnberg, 2003). In this study, the average water content of stabilised clay samples taken from the field was in the range of 64%–66% which corresponds to the average water content of the natural clay (Fig. 4c).

Many researchers (e.g. Carlsten, 1996; Åhnberg, 2003; Baker et al., 2005; Broms, 2004) have reported considerably higher permeability values than those of unstabilised clay. k of stabilised clays with lime-cement admixtures is a function of void ratio (e), the properties of

Table 7
Construction stages used in the FE analysis.

Phase number	Phase	Time interval (days)	Date
0	Initial conditions based on inclinometer readings		2019-06-17
1	Excavation of fill layer	1[c]	2019-06-18
2	Installation of SPW	1[c]	2019-06-19
3	LC column installation	49	2019-08-07
4	Excavation to −2 level	49	2019-09-25
5	Excavation to −7 level	22	2019-10-17
6	Installation of lower strut	21	2019-11-07
7	Excavation to −11 level	17	2019-11-24
8	Dismantling lower strut	52	2020-01-15
9	Last inclinometer readings	32	2020-02-17

[c]Denotes assumption.

pore water and microstructure of pores (sizes and distribution) which are altered during hydration (flocculation, coagulation) and pozzolanic reactions. During pozzolanic reactions, cementation products fill the intra-aggregate pores and k value starts to decrease with increasing lime or cement content (Locat et al., 1996; Quang and Chai, 2015). However, mixing technique (dry/wet), lime/cement ratio, initial properties of in situ clay and the degree of saturation in the field affect the measured permeability. Consequently, the degree of saturation in the field changes with time due to the aforementioned effects.

In this case, IL tests to measure permeability were performed without back pressure for sample saturation. The measured permeability was assumed to be saturated, which, in turn, may result in an overestimation as a decrease in saturation yields a lower unsaturated permeability for stabilised clays due to increasing water sorptivity (Locat et al., 1996; Nguyen et al., 2020). Although the potential investigation of partially saturated permeability presents an intriguing avenue for future research, the analysis relied on the saturated permeability due to a lack of available data on the unsaturated permeability of mixed clay. The degree of saturation in the field undergoes varying changes over time as a result of the micro-structural evolution caused by the flocculation of clay particles and long-term pozzolanic reactions. Due to the heterogeneity of natural clay and the mixing technique, the stabilised clay is also not homogeneous. In the field, there will be fissures and cracks ranging from micro- to macro-scale within LC columns which increase the permeability, thus the permeability measured in the laboratory from laboratory mixed and intact field mixed samples might be used as a lower limit (Åhnberg, 2006).

The difference between the results of the laboratory mixed and field mixed stabilised clay samples can be attributed to the preparation technique of the laboratory mixed samples. On the contrary, the same difference was not seen in c_v profile in Fig. 10(b). The main reason is the high rigidity of the stabilised clay regardless of the sampling type. c_v is a function of the stiffness and the permeability, ergo the dominating parameter would be the stiffness (Larsson and Sällfors, 1996).

4.3. Finite element model and the methodology for simulations

The Central station of the West Link project consists of excavations with different geometries, excavation depths and construction methods. This study focuses on cross-section at KM:456+850 (see Fig. 3).

An eleven-metre-deep braced excavation was supported by sheet pile walls (SPW), two levels of struts, and lime-cement columns constructed utilising the dry mixing method. The finite element analyses were performed using PLAXIS 2D (version 22). The construction sequence was simulated by various phases as presented in Table 7. In the study area, the ground surface corresponds to level +2 before the construction. Struts were installed at levels −0.8 and −6. Before SPW and LC column installation, the 2-m deep fill was excavated, reaching ±0 level. After the fill excavation, SPWs were installed. Later on, in the passive side of the excavation, lime-cement columns were constructed using double overlapping DSM columns (diameter of 70 cm) arranged in a square grid pattern with 2.5 m spacing. The overlap between the columns was 20 cm, resulting in a theoretical area replacement ratio of 66%. The struts at the lower level were dismantled after reaching the final excavation level, in order to allow the construction of the concrete tunnel (Fig. 11).

Table 8
MNhard composite soil parameters using dry soil mixing method.

γ_n (kN/m^3)	G_{50}^{ref} (kPa)	G_{ur}^{ref} (kPa)	p^{ref} (kPa)	m	ϕ'(°)	c' (kPa)	ν'	ν_{ur}
17	20000	50000	100	0.65	37	20	0.25	0.2

A 2D plane strain analysis was performed to simulate the excavation. However, the 3D nature of the problem due to the proximity of a much wider section (see Fig. 2) needs to be kept in mind in the interpretation of the field measurements. The field monitoring data were most likely affected by the adjacent excavation.

Special mesh-dependency study was performed prior to the actual analysis, with mesh refinement around the excavation area where high-stress gradients are expected due to the presence of structural elements, such as lime-cement columns, anchors and SPW. The FE mesh adopted is the outcome of a separate convergence study to ensure mesh-independent results. The high rigidity differences between the in situ clay and stabilised clay necessitated the use of very fine mesh-refinement. The study yielded a final mesh that consists of 2480 15-noded elements and 20269 nodes. The input geometry with the used mesh after the construction of a 1-m thick bottom slab at the end of excavation is shown in Fig. 12.

Standard fixities were applied as displacement boundary conditions. Geometric limits of the boundary value problem were defined based on the guidelines in Lees (2013). Detailed geotechnical site investigations revealed that the soft clay deposit reaches a depth of 55–75 m. Therefore, the hydraulic boundary at the bottom was considered as impermeable. As for the SPW, the wall was also assumed impermeable, and no seepage was allowed through.

Simulation methodology

During the finite element analysis, a simple area ratio calculation was adopted for the improved area by using the methodology described in Broms (2004). The method relies on the use of a weighted average of stiffness modulus. Using the column stiffness (E'_{50}= 85 MPa and E'_{ur}=180 MPa) and the average value of the stiffness along the soft clay profile, where (E'_{50}= 15 MPa and E'_{ur}=39 MPa), the moduli of the homogenised composite material were calculated for a theoretical area replacement ratio of 66% (Eq. (7)). The composite soil was thus modelled using the MNhard soil model with the parameters presented in Table 8.

$$E'_{composite} = 0.66 \times E'_{column} + 0.34 \times E'_{clayavg} \tag{7}$$

Initially, the back analysis was performed excluding the installation effects resulting from LC column construction. The exclusion was simply achieved by adding the total relative displacement at the beginning of the excavation stages to the subsequent inclinometer measurements (Fig. 13).

Fig. 11. The final excavation level of West Link excavation at KM:456+850 (Bozkurt, Sinem. West Link Project, Gothenburg. 16 Feb. 2021. Author's personal collection).

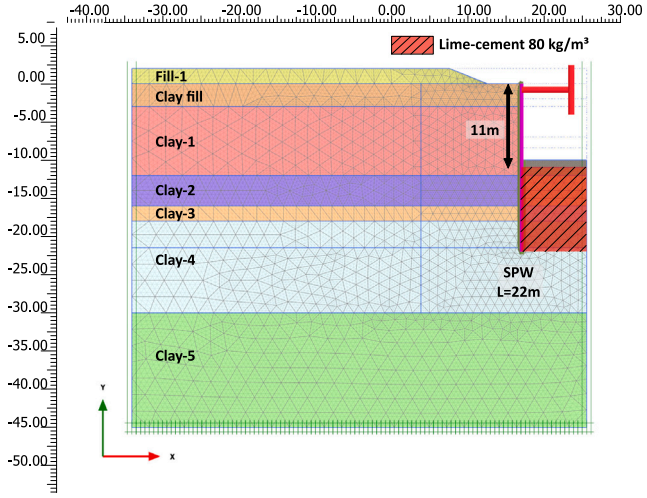

Fig. 12. The FE model of deep excavation at Central Station of West Link project at the end of the excavation.

In Fig. 13a, it is evident that the LC construction results in an expansion with negative horizontal displacements (away from the excavation) corresponding to an order of 50 mm. This magnitude is so high that the exclusion of the installation effects is not a viable approach, as the movements are time-dependent, and this significant amount of expansion was followed by a contraction within the stabilised clay (Fig. 13b). Fig. 13b suggests an additional volumetric strain increment starting from the first excavation stage (excavation to −2 level), with positive values (towards the excavation) reflecting the contraction induced by the dissipation of entrapped air.

In the first back analysis, with the exclusion of the installation effects, the displacements were reset after LC column installation and compared with the adjusted inclinometer readings in Fig. 14. The same time-dependent deformation profile during DSM process can be seen in Fig. 14 more clearly. In the first excavation stage in Fig. 14a, although there is almost no displacement in the FE analysis, inclinometers recorded contraction response with positive values of horizontal displacements (towards the excavation). Therefore, two main mechanisms affecting the simulation were integrated into the back analysis: (1) positive volumetric expansion ($+\varepsilon_v$) resulting from lime-cement column installation and, (2) negative volumetric contraction ($-\varepsilon_v$) induced by consolidation and entrapped air dissipation. The hardening process of the stabilised clay with LC columns was not taken into account in the analysis. The time interval of lime-cement column installation phase, based on construction sequence in field, was defined as 49 days in the simulation. The stiffness of the stabilised clay was computed from the laboratory tests performed on field mixed and laboratory mixed samples, which were either cured in the laboratory for 28 days or taken from the field 21–42 days after the deep mixing. It is important to note that our available data only reflects the properties of the samples at the time they were collected for testing. While the modelling of the curing process holds promise and may be considered in future work, it was assumed that the mixed clay properties represent those at the end of the 28-day curing period. The lateral deformations at the lime-cement column installation were simulated with the aid of varied prescribed strains to accurately capture the inclinometer measurements.

The expansion resulting from the installation of columns was simulated by applying a calibrated constant value of +0.65% additional (expansive) volumetric strain during the installation phase of the columns. In Figs. 13b and 14a, this contraction behaviour is most pronounced down to a depth of −8.5. Although the excavation reaches only a depth of 2-m, the entire wall is moving. Therefore, in order to match the field measurements, an additional calibrated volumetric contraction was applied with the depth-specific average values of −0.40% and −0.15%, respectively. External volumetric strains were applied in the horizontal direction only for the plane strain analysis, and only for the first two phases (LC construction and excavation to −2 level). The simulation of installation effects provided a good replication of the field monitoring data. Note that the provided values of the volumetric strain increments should be considered as site-specific values back-calculated using monitoring data.

The volume change of the stabilised clay can be estimated by the amount of material used in the deep mixing process with Eq. (8) as stated in Swedish Transport Administration (2018).

$$\Delta V_{clay} = 100 \times (w_{binder} \times A)/\gamma_{LC} \tag{8}$$

where ΔV_{clay} represents the volume change of the stabilised clay, w_{binder} is the averaged binder content considering different lime cement ratios utilised (40–80 kg/m^3), A is the area replacement ratio of 0.66 and γ_{LC} is the unit weight of the lime-cement mix (approximately 3200 kg/m^3). Eq. (8) would yield 0.62% expansive strains with the assumption that only horizontal straining occurs. According to calibrated values based on inclinometer readings, roughly half of the expansive volumetric strains approximated the contraction in the stabilised clay. The equation provided above represents a highly rough estimate and does not account for the effect of confining stress along the improvement zone or the existence/dissipation of entrapped air in the pore structure. The deep mixing changes the micro-structure and bonding, aspects that most finite element methods are not capable of incorporating, including mechanical and chemical hydrochemical processes. DSM is highly dependent on workmanship, the properties of in situ soil, and the tools utilised (injection pressure, mixing blade radius, admixture compound, etc.). The volume change can be calculated based on heave

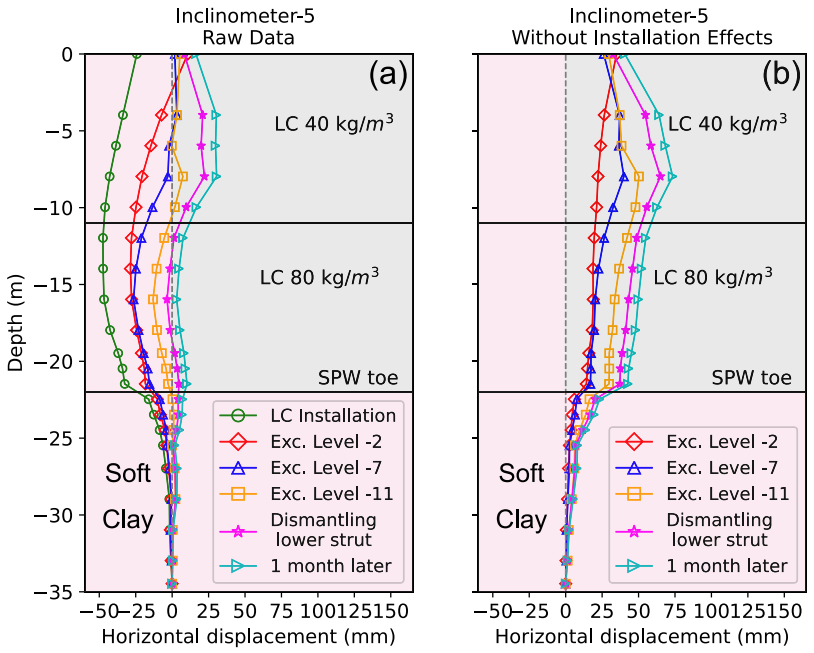

Fig. 13. Measured horizontal displacement from Inclinometer-5 behind SPW. (a) Inclinometer-5 measurements throughout the construction stages (raw data), (b) Inclinometer-5 readings excluding installation effects. Negative values indicate displacement away from the excavation.

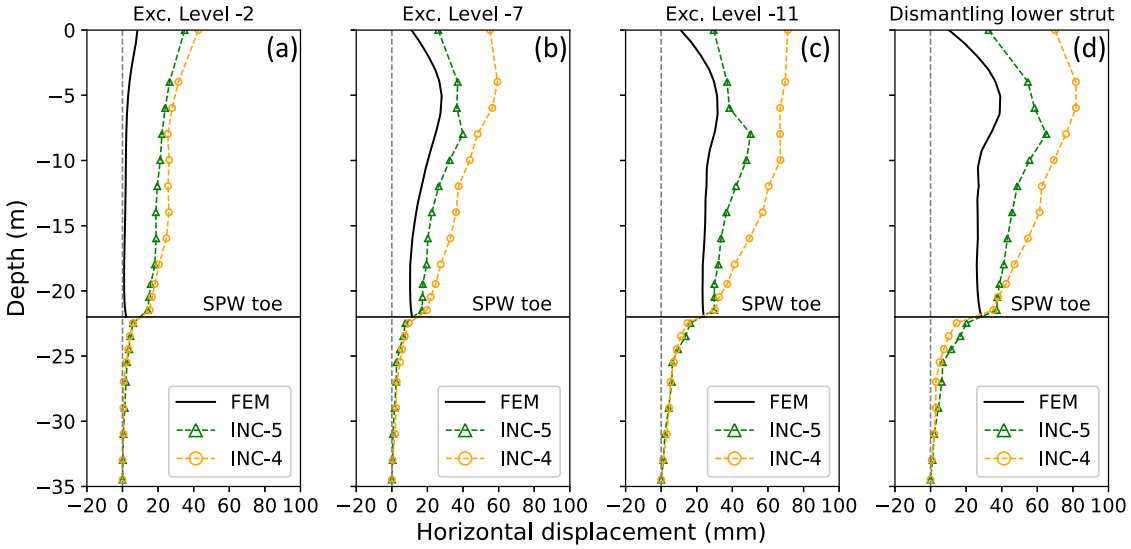

Fig. 14. Horizontal displacement throughout the excavation stages measured from inclinometers and predicted through FE simulation without the installation effects. (a) Excavation to −2 level. (b) Excavation to −7 level. (c) Excavation to −11 level. (d) Reaching final excavation level and dismantling lower strut. Positive values indicate displacement towards the excavation.

and settlement in the passive side of the excavation, starting from the LC column installation for a 28-day curing period. Based on the field observations rough estimates can be revised prior to the excavation.

The simulation considers the temporary excavation before the construction of the concrete tunnel. Neither the variability in LC ratio nor the possible gap between the natural clay and the SPWs were considered. The deformations and pore pressure generation caused by the excavation, the installation of LC columns, struts and anchors, were simulated using FE analysis and compared with the field measurements.

5. Results of finite element analyses and discussion

This section presents a comparison between the FE results and four different types of field measurements: inclinometer readings, pore pressure measurements, surface displacements, captured via prisms, and strain gauges assembled on the struts (strut forces). Fig. 3 shows the locations of the instrumentation and the analysed cross-section.

- *Inclinometer readings*

During the construction period of 8 months, two inclinometers were placed at specific coordinates to monitor the performance of the excavation support system. The results demonstrate that the proximity of the nearby ongoing excavations has a significant effect on the results. The inclinometer indicated with Inc-4, which is close to the adjacent excavation area, yielded higher horizontal deformations than Inc-5. The measurements of Inc-5 are not as sensitive as Inc-4 to adjacent constructions due to its location. Measured deformations in Inc-5 are in accordance with the FE predictions.

A comparison between the simulated results by the fully coupled FE analysis and the monitoring data is presented in Fig. 15 for different

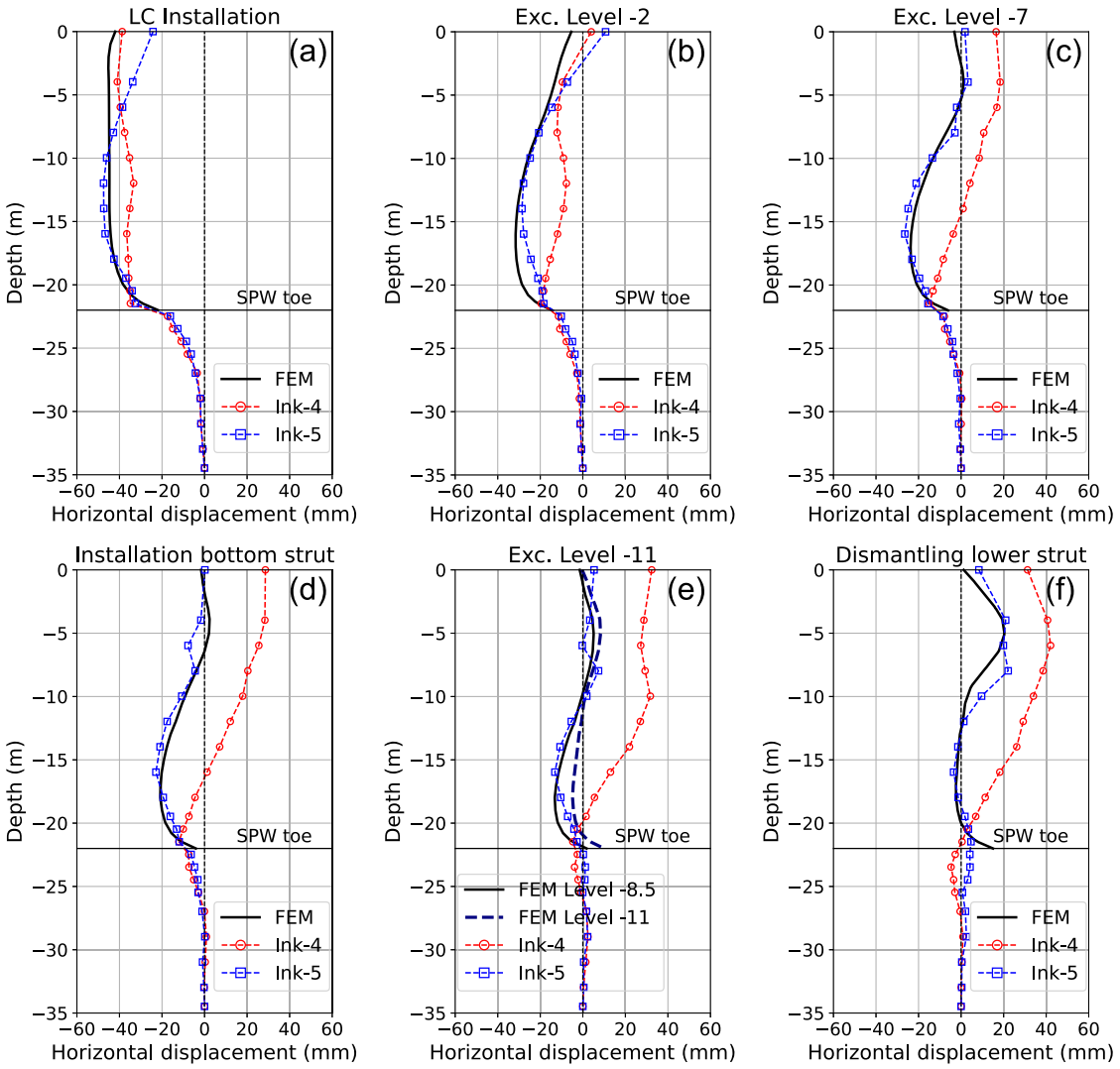

Fig. 15. Comparison of horizontal displacements measured and predicted by FE fully coupled analysis (a) Lime (L)-cement (C) installation. (b) Excavation to −2 level. (c) Excavation to −7 level. (d) Bottom strut installation. (e) Excavation to −11 level. (f) Dismantling bottom strut respectively. Positive values indicate displacement towards the excavation, negative values indicate displacements away from the excavation.

construction stages. Fig. 15a demonstrates that the installation of the LC column changes the initial stress state, and the disturbance of the soil creates large horizontal displacements away from the excavation indicated by negative values. Time-dependent volumetric straining of LC columns took place within 4 months for this specific excavation case history. Inclinometer readings support that the displacements due to the column installation disappeared at the onset of the excavation stages.

The recorded horizontal displacement values of the far-field inclinometer (Inc-5) versus the FE results are plotted in Fig. 16 throughout the construction period. In Fig. 16, the difference between the recorded data below the pile tip (at the depth of 24.5 m) versus the FE analysis stems from the assumptions with regard to the installation of inclinometers. Normally the interpretation of the inclinometer readings relies on the assumption that horizontal movements at the bottom of the inclinometer tube would be restricted or of negligible magnitude. Due to the application of grouting at the lowermost part, no movement can be detected. This is particularly problematic when a bearing stratum is absent. In soft clays, the floating inclinometer probe tends to settle and displace horizontally according to the direction of the movement of the excavation. In some cases, displacements in two directions account for the measured tilt. Therefore, horizontal displacements especially for the lowermost part may not be captured.

As described in Section 4.3, no additional volumetric strain application was made after the excavation stage down to the −2 level. the progress in the excavation led to a change in the horizontal displacement profile. The direction of the displacements changed towards the excavation, with positive values. Considering the general trend, the FE simulations were able to capture the field response well.

The calculated and measured horizontal displacements are in the order of 20 mm at the end of the excavation after the dismantling of the lower strut. The ratio between the maximum lateral wall deformation and excavation depth (δ_x/H_e) is of 0.2%. In this study, ignoring installation effects would yield δ_x/H_e ratio of 0.4%. The expansion owing to column installation resulted in significant lateral displacements away from the excavation. δ_x/H_e reduced by about 50% at the end of final excavation. According to data acquired worldwide, problems had been recorded when the lateral displacement and excavation ratio was higher than 0.3% (Long, 2001). PSCG (2000) database presents deformation control criteria for the excavations in soft soils based on the presence of significant infrastructure in the vicinity and/or buildings in use within a distance of 1–2 excavation depth (H_e), and defines the allowable displacement as 0.3%H_e. The most common procedure in conventional design is to ignore installation effects. Considering the excavation was completed without any major problems, neglecting

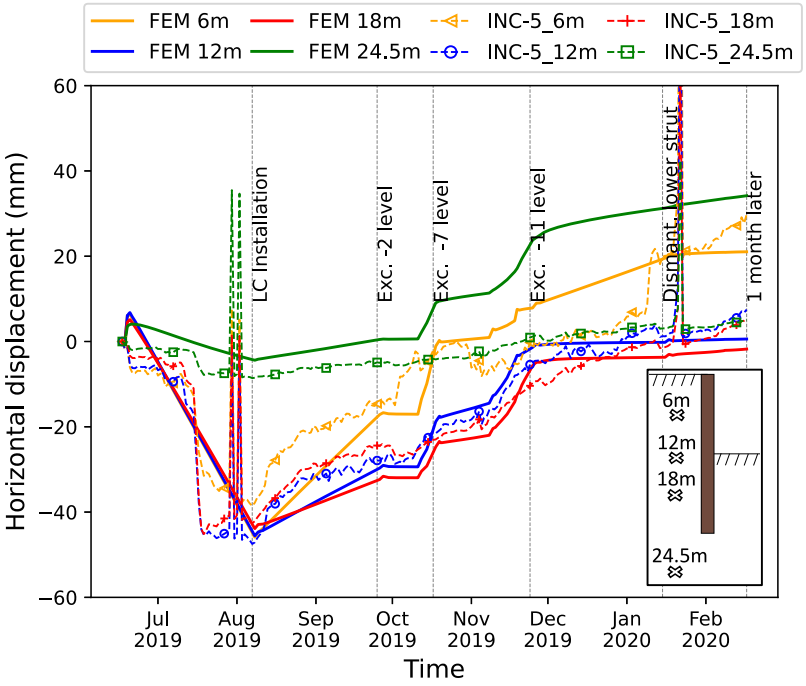

Fig. 16. Measured versus calculated horizontal displacement behind SPW. Positive values indicate displacement towards the excavation.

Table 9
Distance of pore pressure measurement stations to West Link E02 deep excavation.

Station No	Depth (m)	Distance to the SPWs (m)
P1	8 16 24	≈0.5
P2	8 18 28	≈10.5

Table 10
Distance of surface displacement prisms to the SPWs.

Prism no	Distance to the SPWs (m)
SP3030	≈0.5
SP3005	≈0.5
B3001	≈10
B3002	≈10
MP3003	≈10
MP4002	≈10
EL3001	≈20

the installation effects might lead to expensive and over-conservative designs.

- *Pore pressures*

The pore pressure probes were installed at specific locations as indicated in Table 9. The results of the FE analyses with respect to the field monitoring data are presented in Fig. 17.

The calculated pore water pressures are in good agreement with the field measurements, except for the deep clay layers (below 18 m). The analyses were performed both with and without the installation effects to study the pore pressure build-up. The application of external volumetric strains to simulate the expansion and contraction characteristics of LC columns had a marginal effect on the pore pressure generation. The application of volumetric strains thus mostly affected the deformation profile of the braced excavation system.

The results of the FE analysis do not reflect the pore pressure measurements near the SPWs, especially for the deep layers. High vertical and confining stresses in deep layers might lead to leakage from weak joins within SPWs. Although SPWs were considered impermeable in the simulations, leakage from the joints can occur in the field. Such a phenomenon was noticed during site visits (Fig. 18). The leakage from the joints shown most likely occurred within the highly heterogeneous fill layer which probably contains a significant amount of granular material.

- *Prisms*

During the construction period, several surface displacement prisms were placed approximately 0.5 m, 10 m and 20 m away from the excavation (Table 10). The horizontal and vertical displacement profiles calculated with the FE analysis conform with the monitoring data (Fig. 19). It is evident that the heave mechanism reduced with the progress in the excavation (Fig. 19a). The heave behind the SPWs was prevailing at a distance of 10 m with a maximum value of 75 mm behind the SPW.

Field monitoring data, especially for the surface readings should be interpreted cautiously, as displacement gauges are sensitive to physical activities involving surcharge load due to ongoing constructions and nearby excavation facilities. Indeed, the discontinuities in the data can be attributed to the effects of these activities, independent of the actual excavation.

- *Strain gauges assembled on struts (strut forces)*

Throughout the construction period, axial forces acting on the struts were recorded via strain gauges. The gauges were assembled on two sections on the upper struts: at the middle of the span and at a distance of 3 m from the corners. The section of the installation was at a distance of 3 m from the corners for the lower struts. The measurements were made in four different locations: 1, 2, 3 and 4 (Fig. 20).

The nature of the excavation problem involves 3D effects, which are not possible to be captured with 2D analysis. The excavation activities in the vicinity of the study area are a direct contributor to the differences between field measurements and the results of the simulation. The maximum axial force distribution of the mid-span forces could not be captured with 2D simulations on account of simplifications made in strut spacing. In the plane strain analysis, the average values of the

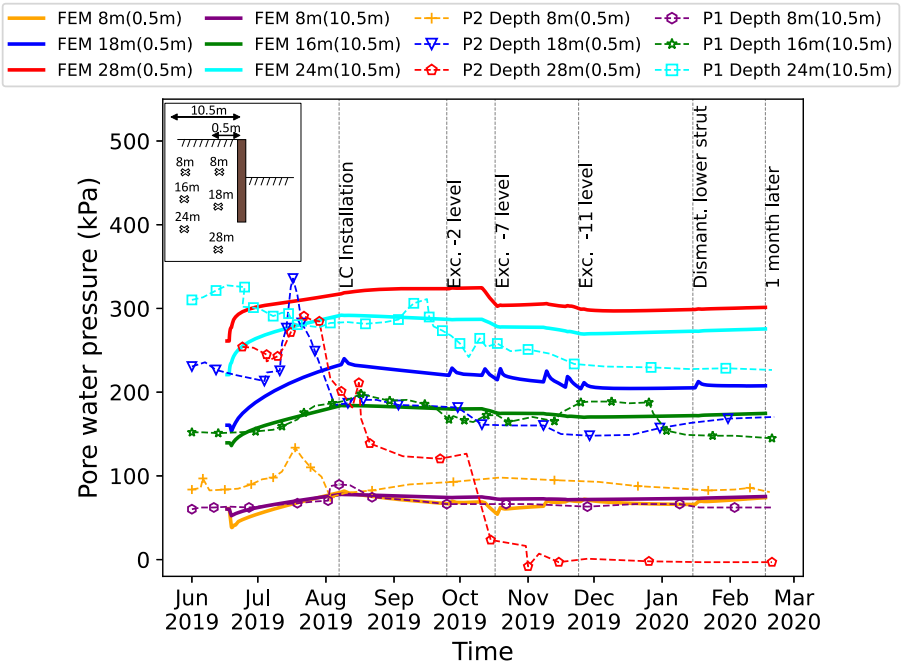

Fig. 17. Monitoring data versus predicted pore pressures.

Fig. 18. Leakage from the joints of SPW (Bozkurt, Sinem. West Link project, Gothenburg. 16 Feb. 2021. Author's personal collection).

strut spacings were utilised. Therefore, according to the FE analysis, the maximum forces calculated for the upper struts were similar to those of the field measurements of *Strut 1* (see Fig. 21a). *Strut 2* was probably not exposed to a high force distribution unlike *Strut 1*, owing to the variation in the spacing. The same consideration is valid for the lower strut forces. The axial force distribution of *Strut 4* was in accordance with the results of the FE calculation for the lower struts (see Fig. 21b).

It is worth mentioning that the same analyses were also performed without the application of additional volumetric strain to simulate installation effects. The results yielded the same values for the axial force profile acting on the struts. Fluctuations in the recorded axial force distribution of the monitoring data can be attributed to temperature effects and time differences during strut installation which were not accounted for in this study.

6. Conclusions

Fully coupled two-dimensional finite element analyses of a braced excavation supported by lime-cement columns were performed, and the results were compared to the field monitoring data. Due to the lack of a straightforward procedure for the quantitative assessment of the mixing-related installation effects, back analyses were performed by making use of the inclinometer readings at the early stage of construction. The prescribed volumetric strain application was utilised to simulate the deformations caused by the dry soil mixing process.

The numerical analyses were carried out with and without the inclusion of installation effects in order to demonstrate the extent to which the process of lime-cement column stabilisation influences the stress–strain response. The forces in the structural elements and the pore pressure distribution as well as the overall time-dependent deformation behaviour over an 8-month period were replicated with reasonable accuracy by taking account of the installation effects. The ratio between the maximum lateral displacement and the excavation height was reduced by about 50% when taking into account the installation effects, compared to the analysis without the inclusion of installation effects. The maximum lateral displacement calculated in each construction stage was of the same order as recorded in the field. Therefore, incorporating the effect of lime-cement construction into the traditional design would provide cost-effective and realistic designs. However, the generalisation of the strain application needs further investigation. The adopted values of the volumetric strain in this study should be regarded as case history-specific values.

The laboratory tests on both laboratory-mixed and field-mixed samples indicated that the rheological properties of the stabilised clay might be affected by various factors including the engineering properties of in situ clay and deep mixing procedure. Furthermore, the field performance of lime-cement stabilisation relies largely on the success of the construction (homogeneity as well as achieving the design strength and stiffness in the field). Consequently, conducting a reliability assessment of the support system becomes necessary to evaluate the influence of the variability of the stabilised soil, specifically in terms of stiffness, on deformation and structural forces. In this regard, primarily global sensitivity analyses (Tahershamsi and Dijkstra, 2022) can be performed to identify the most influential parameters affecting the support system. Subsequently, stochastic variability of the stabilised clay can be incorporated in the finite element analyses with the use of a random sampling technique, such as Monte Carlo simulations.

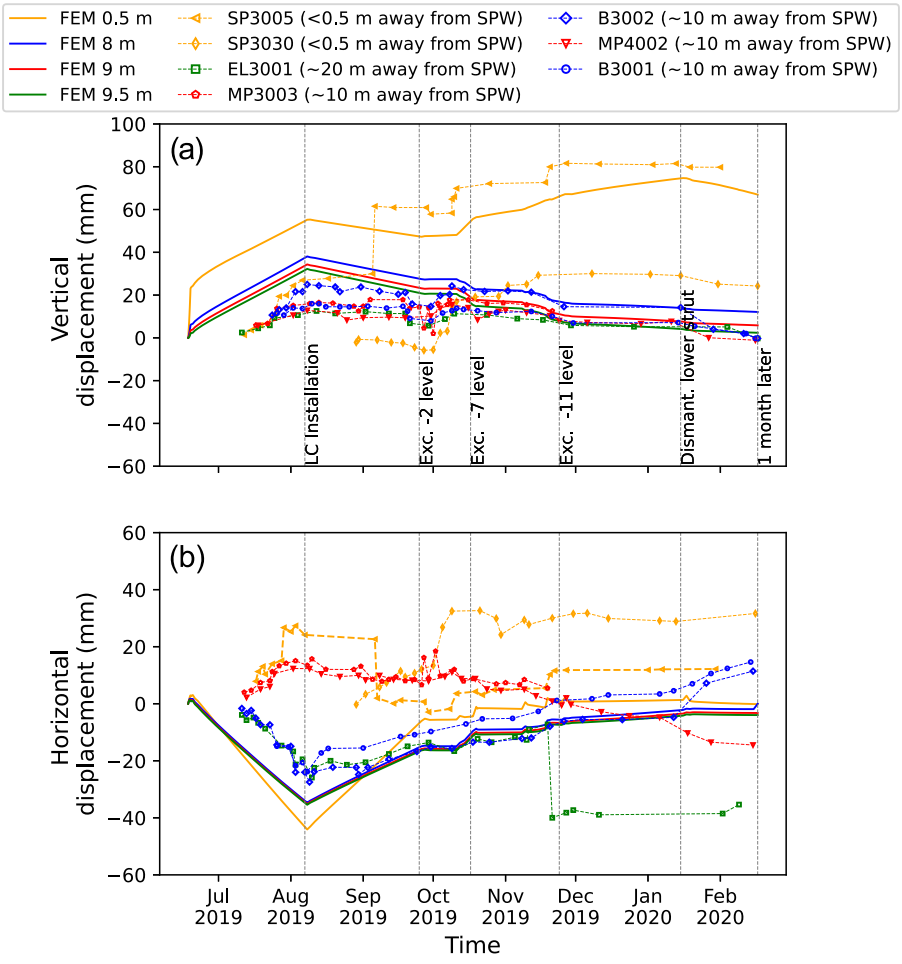

Fig. 19. Monitoring data versus predicted vertical (a) and horizontal (b) displacement profile. Positive values of vertical and horizontal displacement indicate heave and displacement towards excavation, respectively.

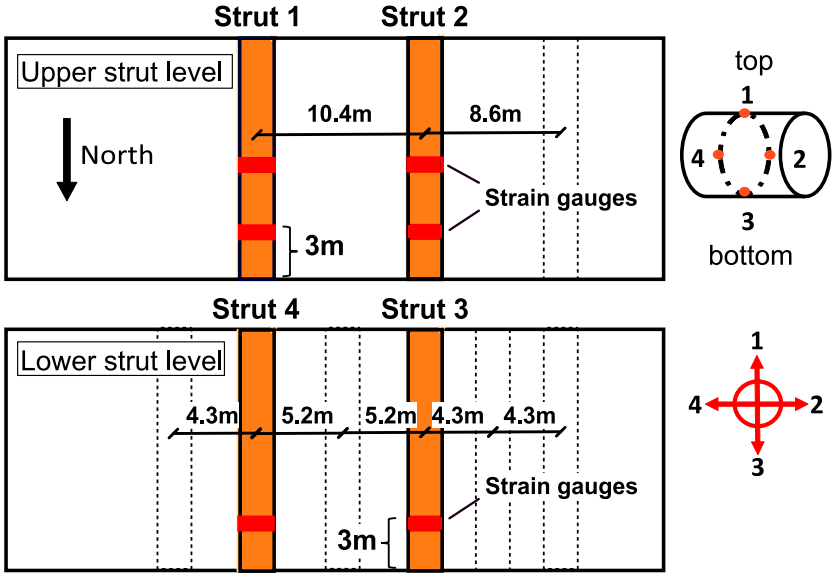

Fig. 20. The location of the strain gauges assembled on struts.

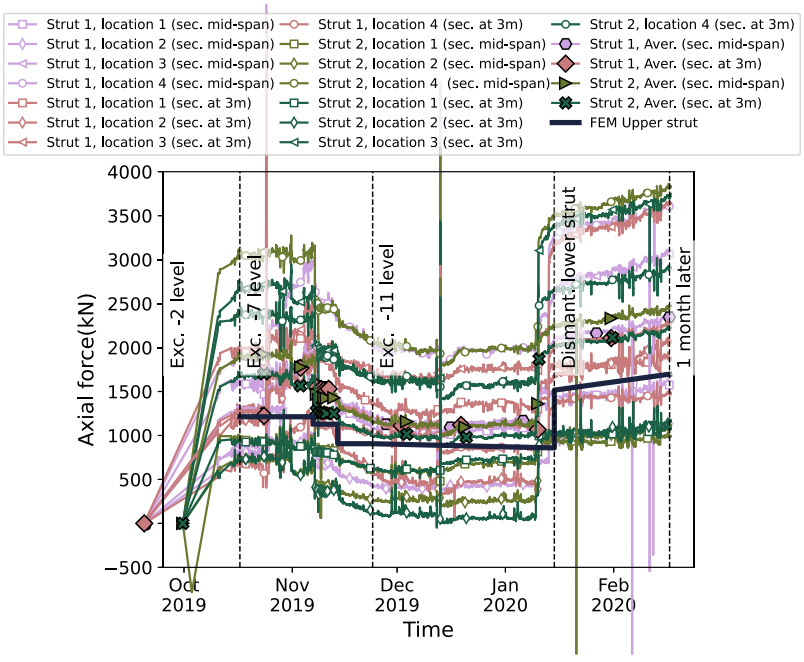

(a) Monitoring data versus predicted upper strut force.

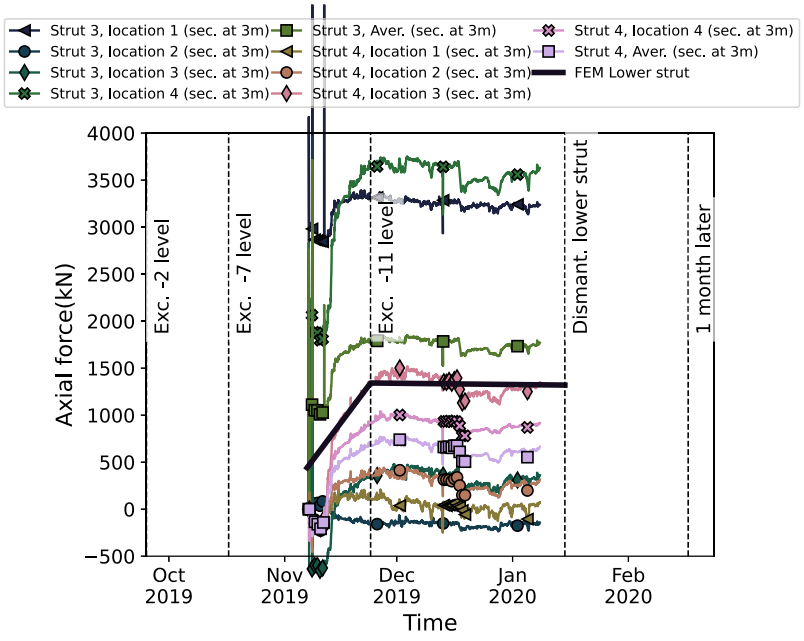

(b) Monitoring data versus predicted lower strut force.

Fig. 21. Comparison of monitored and predicted strut forces for (a) upper and (b) lower struts.

CRediT authorship contribution statement

Sinem Bozkurt: Conceptualization, Methodology, Formal analysis, Writing – original draft, Visualization. **Ayman Abed:** Supervision, Review & editing. **Minna Karstunen:** Supervision, Review & editing.

Declaration of competing interest

The authors declare that they have no known competing financial interests or personal relationships that could have appeared to influence the work reported in this paper.

Data availability

The authors do not have permission to share data.

Acknowledgements

The work was benefitting from financial support by BIG (Better Interaction in Geotechnics, Grant 2020/46703, from the Swedish Transport Administration (TRV)) and the Swedish Research Council for Sustainable Development (Formas Grant 2019-00456). The work is done as a part of the Digital Twin Cities Centre supported by Sweden's Innovation Agency VINNOVA (Grant 2019-00041). The authors would also like to thank Jonatan Isaksson from NCC AB for providing access to the field measurements.

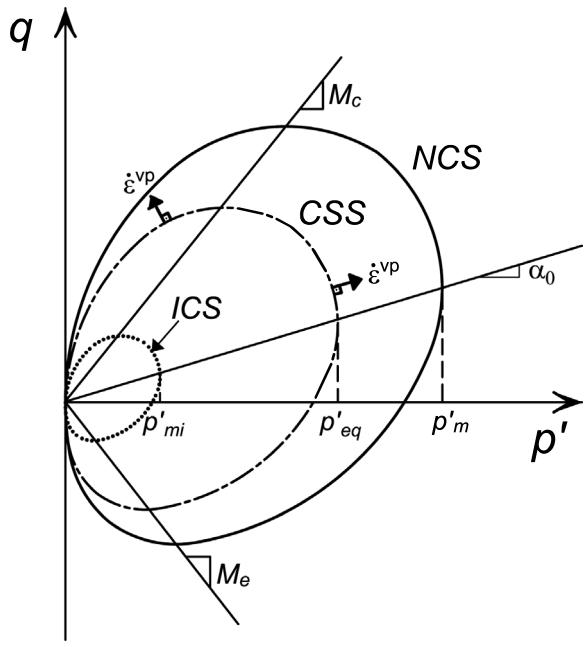

Fig. A.22. Creep SCLAY1S model normal consolidation surface (NCS), current stress surface (CSS) and intrinsic compression surface (ICS) in triaxial stress space.

Appendix A. Creep-SCLAY1S model

The complete formulation of the Creep-SCLAY1S can be found in Sivasithamparam et al. (2015), Gras et al. (2018) but it is summarised here. The various surfaces of the Creep-SCLAY1S are visualised in Fig. A.22 in triaxial stress space. The equation for the Normal Compression Surface (NCS), which represents the boundary between large and small creep strains, can be expressed in the simplified form of triaxial space with Eq. (A.1) and in 3D stress space with Eq. (A.2):

$$f_{NCS} = (q - \alpha p')^2 - (M(\theta)^2 - \alpha^2)(p'_m - p')p' = 0 \tag{A.1}$$

$$f_{NCS3D} = \underbrace{\frac{3}{2}\left(\{\sigma'_d - p'\alpha_d\}^T \{\sigma'_d - p'\alpha_d\}\right)}_{q^2} - \left(M(\theta)^2 - \underbrace{\frac{3}{2}\{\alpha_d\}^T\{\alpha_d\}}_{\alpha^2}\right)\times (p'_m - p')\,p' = 0 \tag{A.2}$$

where $q^2 = \sqrt{3/2\left(\{\sigma'_d - p'\alpha_d\}^T \{\sigma'_d - p'\alpha_d\}\right)}$ is the scalar value of the modified deviatoric stress tensor, including anisotropy represented by a deviatoric fabric tensor α_d. $q = (\sigma'_1 - \sigma'_3)$ in triaxial stress space. Mean effective stress is $p' = (\sigma'_1 + \sigma'_2 + \sigma'_3)/3$ and the vertical tangent to NCS designates the size or NSC in the isotropic axis, p'_m. $M(\theta)$ represents the Lode angle-dependent stress ratio at critical state. The subscript NCS denotes the Normal Compression Surface (NCS), and α represents the scalar value of the fabric tensor, defined as $\alpha^2 = \sqrt{3/2\left({\alpha_d}^T : \alpha_d\right)}$, which describes the orientation of the model surfaces, as illustrated in triaxial stress space in Fig. A.22. The deviatoric stress tensor and deviatoric fabric tensor are expressed by Eqs. (A.3) and (A.4).

$$\sigma'_d = \begin{bmatrix} \sigma'_x - p' \\ \sigma'_y - p' \\ \sigma'_z - p' \\ \sqrt{2}\tau_{xy} \\ \sqrt{2}\tau_{yz} \\ \sqrt{2}\tau_{zx} \end{bmatrix} \tag{A.3}$$

Table B.11
Rigidity parameters of the structural elements.

	Sheet pile walls (AZ-38-700N)	Upper strut	Lower strut	Unit
Material type	Elastoplastic	Elastic	Elastic	–
EA_1	4.83E6	0.64E6	1.57E6	kN/m
EA_2	0.24E6	0.64E6	1.57E6	kN/m
EI	0.20E6	–	–	kNm^2/m
d	0.70	–	–	m
w	1.808	–	–	kN/m/m
M_p	1046	–	–	kN/m/m
N_p, 1	5520	–	–	kN/m
N_p, 2	276	–	–	kN/m
σ_{yield}	240000	–	–	kN/m^2

$$\alpha_d = \begin{bmatrix} \frac{1}{3}\left((2\alpha_x - \alpha_y - \alpha_z)\right) \\ \frac{1}{3}\left((-\alpha_x + 2\alpha_y - \alpha_z)\right) \\ \frac{1}{3}\left((-\alpha_x - \alpha_y + 2\alpha_z)\right) \\ \sqrt{2}\alpha_{xy} \\ \sqrt{2}\alpha_{yz} \\ \sqrt{2}\alpha_{zx} \end{bmatrix} with\ \frac{1}{3}\left(\alpha_x + \alpha_y + \alpha_z\right) = 1 \tag{A.4}$$

The rate-dependency is represented by the concept of a constant rate of visco-plastic multiplier (Eq. (A.5) based on Grimstad et al. (2010).

$$\dot{\Lambda} = \frac{\mu_i^*}{\tau}\left(\frac{p'_{eq}}{p'_m}\right)^{\beta}\left(\frac{\left(M_c^2 - \alpha^2_{K_0^{NC}}\right)}{\left(M_c^2 - \eta^2_{K_0^{NC}}\right)}\right) with\ \beta = \left(\frac{\lambda_i^* - \kappa^*}{\mu_i^*}\right) \tag{A.5}$$

Deviatoric and volumetric components of creep strains can thus be calculated as follows:

$$\dot{\varepsilon}_v^c = \dot{\Lambda}\frac{\partial p'_{eq}}{\partial p'} \ and\ \dot{\varepsilon}_q^c = \dot{\Lambda}\frac{\partial p'_{eq}}{\partial q} \tag{A.6}$$

The size of the intrinsic consolidation surface (ICS) is assumed to be dependent only on volumetric creep strains, ε_v^c.

$$\dot{p}'_{mi} = p'_{mi}\exp\left(\frac{\dot{\varepsilon}_v^c}{\lambda_i^* - \kappa^*}\right) \tag{A.7}$$

The evolution of the size of p'_m, corresponding to the current degree of bonding (χ), and the degradation of bonding are calculated with Eq. (A.8)

$$\dot{\chi} = -a\chi\left(|\,\dot{\varepsilon}_v^c\,| + b\,|\,\dot{\varepsilon}_d^c\,|\right) \ and\ \dot{p}_m = p_{mi}(1 + \dot{\chi}) \tag{A.8}$$

The evolution of anisotropy is described with Eq. (A.9) in 3D stress space.

$$\dot{\alpha} = \omega\left[\left(\frac{3\sigma'_d}{4p'} - \alpha_d\right)\langle\dot{\varepsilon}_v^c\rangle + \omega_d\left(\frac{\sigma'_d}{3p'} - \alpha_d\right)\dot{\varepsilon}_d^c\right] \tag{A.9}$$

Appendix B. Structural element parameters

The rigidity parameters of the structural elements used in the analysis are given in Table B.11. I is the moment of inertia, w is the specific unit weight, d is the (equivalent) thickness, $N_{p,1}$ and $N_{p,2}$ are the maximum axial forces in the 1-direction (in-plane) and 2-direction (out of plane), respectively. M_p expresses the maximum bending moment and σ_{yield} denotes the yield strength of steel. EA_1 and EA_2 define the normal elastic stiffnesses of the SPWs in the 1-direction and 2-direction, respectively, where E is the elastic modulus of the steel and A is the section area.

Appendix C. CRS tests performed on soft clay samples

Constant rate of strain (CRS) oedometer tests were carried out with drainage to the upper boundary of the sample, and pore pressures were measured at the base. The results of the CRS tests performed on

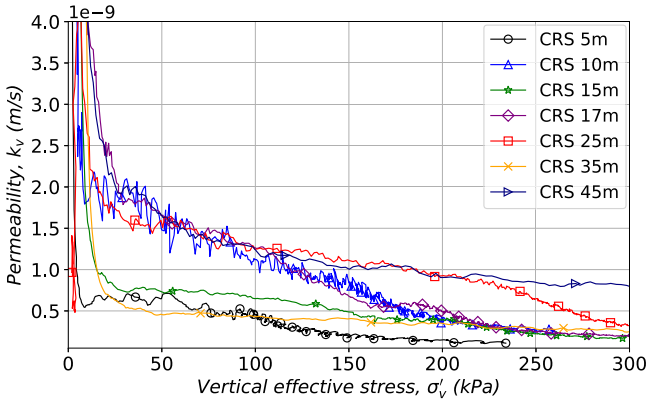

Fig. C.23. CRS tests on soft clay samples.

the soft clay samples, taken from seven different depths in the site, were presented in Fig. C.23. In the finite element analysis, k values corresponding to preconsolidation stress were utilised.

References

Åhnberg, H., 2003. Measured permeabilities in stabilized Swedish soils. In: Grouting and Ground Treatment. pp. 622–633. http://dx.doi.org/10.1061/40663(2003)34.

Åhnberg, H., 2006. Strength of stabilised soils – A laboratory study on clays and organic soils stabilised with different types of binder. URL: www.swedgeo.se.

Åhnberg, H., Bengtsson, P.E., Holm, G., 2001. Effect of initial loading on the strength of stabilised peat. Proc. Inst. Civ. Eng. Ground Improv. 5, 35–40. http://dx.doi.org/10.1680/grim.2001.5.1.35.

Baker, S., Sällfors, G., Alén, C., 2005. Deformation properties of lime/cement columns. evaluation from in-situ full scale tests of stabilised clay. In: Deep Mixing'05.

Benz, T., 2007. Small-Strain Stiffness of Soils and Its Numerical Consequences. Volume 5. Univ. Stuttgart, Inst. f. Geotechnik Stuttgart.

Benz, T., Wehnert, M., Vermeer, P.A., 2008. A lode angle dependent formulation of the hardening soil model. In: 12th International Conference on Computer Methods and Advances in Geomechanics 2008. pp. 653–660.

Black, D.K., Lee, K.L., 1973. Saturating laboratory samples by back pressure. ASCE J. Soil Mech. Found. Div. 99, 75–93. http://dx.doi.org/10.1061/jsfeaq.0001847.

Broms, B., 1999. Can lime/cement columns be used in Singapore and Southeast Asia? In: 3rd GRC Lecture. Nanyang Technological University and NTU-PWD Geotechnical research Centre, Singapore, p. 214.

Broms, B., 2004. Lime and lime/cement columns. Ground Improv. 2, 252–330.

Bruce, M.E.C., Berg, R.R., Filz, G.M., Terashi, M., Yang, D.S., Collin, J.G., Geotechnica, S., et al., 2013. Federal Highway Administration Design Manual: Deep Mixing for Embankment and Foundation Support (No. FHWA-HRT-13-046). Technical Report, Federal Highway Administation. Offices of Research & Development, United States.

Carlsten, P., 1996. Lime and lime/cement columns. Dev. Geotech. Eng. 80, 355–399. http://dx.doi.org/10.1016/S0165-1250(96)80013-7, (Chapter 10).

CEN, 2005. Execution of Special Geotechnical Works – Deep Mixing (EN14679:2005). European Standard, European Commitee for Standardization.

Chew, S.H., Kamruzzaman, A.H.M., Lee, F.H., 2004. Physicochemical and engineering behavior of cement treated clays. J. Geotech. Geoenviron. Eng. 130, 696–706. http://dx.doi.org/10.1061/(ASCE)1090-0241(2004)130:7(696).

Clough, G.W., Asce, M., Hansen, L.A., Asce, A.M., 1981. Clay anisotropy and braced wall behavior. J. Geotech. Eng. Div. 107, 893–913. http://dx.doi.org/10.1061/AJGEB6.0001168, URL: https://ascelibrary.org/doi/abs/10.1061/AJGEB6.0001168.

Consoli, N.C., Da Silva Lopes, L., Consoli, B.S., Festugato, L., 2014. Mohr–Coulomb failure envelopes of lime-treated soils. Geotechnique 64, 165–170. http://dx.doi.org/10.1680/geot.12.P.168, URL: https://www.icevirtuallibrary.com/doi/abs/10.1680/geot.12.P.168.

Eigenbrod, K.D., 1975. Analysis of the pore pressure changes following the excavation of a slope. Can. Geotech. J. 12, 429–440.

Finno, R.J., Nerby, S.M., 1989. Saturated clay response during braced cut construction. J. Geotech. Eng. 115, 1065–1084. http://dx.doi.org/10.1061/(ASCE)0733-9410(1989)115:8(1065).

Ghadrdan, M., Shaghaghi, T., Tolooiyan, A., 2020. Effect of negative excess pore-water pressure on the stability of excavated slopes. Géo. Lett. 10, 20–29. http://dx.doi.org/10.1680/jgele.19.00040.

Graham, J., Houlsby, G., 1983. Anisotropic elasticity of a natural clay. Géotechnique 33, 165–180.

Gras, J.P., Sivasithamparam, N., Karstunen, M., Dijkstra, J., 2017. Strategy for consistent model parameter calibration for soft soils using multi-objective optimisation. Comput. Geotech. 90, 164–175. http://dx.doi.org/10.1016/J.COMPGEO.2017.06.006.

Gras, J.P., Sivasithamparam, N., Karstunen, M., Dijkstra, J., 2018. Permissible range of model parameters for natural fine-grained materials. Acta Geotech. 13, 387–398. http://dx.doi.org/10.1007/S11440-017-0553-1/TABLES/3.

Grimstad, G., Degago, S.A., Nordal, S., Karstunen, M., 2010. Modeling creep and rate effects in structured anisotropic soft clays. Acta Geotech. 5, 69–81. http://dx.doi.org/10.1007/S11440-010-0119-Y/FIGURES/17.

Holm, G., 2003. State of practice in dry deep mixing methods. In: Grouting and Ground Treatment. pp. 145–163. http://dx.doi.org/10.1061/40663(2003)5, URL: https://ascelibrary.org/doi/abs/10.1061/40663%282003%295.

Horpibulsuk, S., Miura, N., Nagaraj, T.S., 2003. Assessment of strength development in cement-admixed high water content clays with abrams' law as a basis 53. pp. 439–444. http://dx.doi.org/10.1680/GEOT.2003.53.4.439.

Ignat, R., Baker, S., Holmén, M., Larsson, S., 2019. Triaxial extension and tension tests on lime-cement-improved clay. Soils Found. 59, 1399–1416. http://dx.doi.org/10.1016/j.sandf.2019.06.004, URL: https://linkinghub.elsevier.com/retrieve/pii/S0038080619301143.

Ignat, R., Baker, S., Karstunen, M., Liedberg, S., Larsson, S., 2020. Numerical analyses of an experimental excavation supported by panels of lime-cement columns. Comput. Geotech. 118, 103296. http://dx.doi.org/10.1016/j.compgeo.2019.103296, URL: https://linkinghub.elsevier.com/retrieve/pii/S0266352X1930360X.

Ignat, R., Baker, S., Liedberg, S., Larsson, S., 2016. Behavior of braced excavation supported by panels of deep mixing columns. Can. Geotech. J. 53, 1671–1687. http://dx.doi.org/10.1139/cgj-2016-0137, URL: http://www.nrcresearchpress.com/doi/10.1139/cgj-2016-0137.

Jamsawang, P., Boathong, P., Mairaing, W., Jongpradist, P., 2016. Undrained creep failure of a drainage canal slope stabilized with deep cement mixing columns. Landslides 13, 939–955. http://dx.doi.org/10.1007/S10346-015-0651-9/FIGURES/21, URL: https://link.springer.com/article/10.1007/s10346-015-0651-9.

Jamsawang, P., Voottipruex, P., Boathong, P., Mairaing, W., Horpibulsuk, S., 2015. Three-dimensional numerical investigation on lateral movement and factor of safety of slopes stabilized with deep cement mixing column rows. Eng. Geol. 188, 159–167. http://dx.doi.org/10.1016/J.ENGGEO.2015.01.017.

Karstunen, M., Koskinen, M., 2008. Plastic anisotropy of soft reconstituted clays. Can. Geotech. J. 45, 314–328. http://dx.doi.org/10.1139/T07-073, URL: https://cdnsciencepub.com/doi/abs/10.1139/T07-073.

Karstunen, M., Krenn, H., Simon, Wheeler, J., Koskinen, M., Zentar, R., 2005. Effect of anisotropy and destructuration on the behavior of murro test embankment. Int. J. Geomech. 5, 87–97. http://dx.doi.org/10.1061/(ASCE)1532-3641(2005)5:2(87).

Kavvadas, M., Amorosi, A., 2000. A constitutive model for structured soils. Géotechnique 50, 263–273. http://dx.doi.org/10.1680/geot.2000.50.3.263.

Kawasaki, T., 1981. Deep mixing method using cement hardening agent. In: Proc. of 10th Int. Conf. on SMFE. pp. 721–724.

Kitazume, M., Maruyama, K., 2006. External stability of group column type deep mixing improved ground under embankment loading. Soils Found. 46, 323–340. http://dx.doi.org/10.3208/sandf.46.323, URL: https://www.sciencedirect.com/science/article/pii/S0038080620305618.

Krenn, H., Karstunen, M., 2008. Numerical modelling of deep mixed columns below embankments constructed on soft soils. In: Proceedings of the 2nd International Workshop on Geotechnics of Soft Soils. pp. 159–164.

Lambe, T.W., Whitman, R.V., 1969. Soil Mechanics. John Wiley & Sons.

Larsson, S., 2003. Mixing Processes for Ground Improvement by Deep Mixing (Ph.D. thesis). Byggvetenskap.

Larsson, S., 2017. The mixing process at the dry jet mixing method. In: Dry Mix Methods for Deep Soil Stabilization. Routledge, pp. 339–346.

Larsson, R., Sällfors, G., 1996. Automatic continuous consolidation testing in sweden, consolidation of soils. ASTM, STP 892, 229–238.

Lees, A., 2013. Geotechnical Finite Element Analysis. ICE publishing.

Leoni, M., Karstunen, M., Vermeer, P.A., 2008. Anisotropic creep model for soft soils. Geotechnique 58, 215–226. http://dx.doi.org/10.1680/geot.2008.58.3.215.

Leroueil, S., Kabbaj, M., Tavenas, F., Bouchard, R., 1985. Stress–strain-strain rate relation for the compressibility of sensitive natural clays. Geotechnique 35, 159–180. http://dx.doi.org/10.1680/geot.1985.35.2.159.

Locat, J., Tremblay, H., Leroueil, S., 1996. Mechanical and hydraulic behaviour of a soft inorganic clay treated with lime. Can. Geotech. J. 33, 654–669. http://dx.doi.org/10.1139/T96-090-311.

Long, M., 2001. Database for retaining wall and ground movements due to deep excavations. J. Geotech. Geoenviron. Eng. 127, 203–224. http://dx.doi.org/10.1061/(ASCE)1090-0241(2001)127:3(203).

Lorenzo, G.A., Bergado, D.T., 2006. Fundamental characteristics of cement-admixed clay in deep mixing. J. Mater. Civ. Eng. 18, 161–174. http://dx.doi.org/10.1061/(ASCE)0899-1561(2006)18:2(161).

Marte, R., Scharinger, F., Lüftenegger, R., 2017. Panels made by the deep mixing method for a building pit support in a slope. pp. 385–394. http://dx.doi.org/10.1061/9780784480809.037.

Matsuoka, H., Nakai, T., 1974. Stress-deformation and strength characteristics of soil under three different principal stresses. In: Proceedings of the Japan Society of Civil Engineers. Japan Society of Civil Engineers, pp. 59–70.

Matsuoka, H., Nakai, T., 1982. A new failure criterion for soils in three dimensional stresses. In: IUTAM Conference on Deformation and Failure of Granular Materials. Delft, pp. 253—-263.

Nguyen, T., Cui, Y., Tang, A., Herrier, G., V, F., Mauduit, C., Plier, F., 2020. Evaluation of the method of determining unsaturated hydraulic conductivity based on the pore size distribution curve. Unsaturated Soils Res. Appl. 114, 3–1148. http://dx.doi.org/10.1201/9781003070580-32.

Oates, J.A.H., 2008. Lime and Limestone: Chemistry and Technology, Production and Uses. John Wiley & Sons.

Olsson, M., 2013. On Rate-Dependency of Gothenburg Clay (Ph.D. thesis). Chalmers University of Technology, URL: https://research.chalmers.se/en/publication/185175.

O'Rourke, T.D., O'Donnell, C.J., 1997. Field behavior of excavation stabilized by deep soil mixing. J. Geotech. Geoenviron. Eng. 123, http://dx.doi.org/10.1061/(asce)1090-0241(1997)123:6(516).

Ou, C.Y., Teng, F.C., Wang, I.W., 2008. Analysis and design of partial ground improvement in deep excavations. Comput. Geotech. 35, 576–584. http://dx.doi.org/10.1016/J.COMPGEO.2007.09.005.

Pande, G.N., Sharma, K.G., 1983. Multi-laminate model of clays—a numerical evaluation of the influence of rotation of the principal stress axes. Int. J. Numer. Anal. Methods Geomech. 7, 397–418. http://dx.doi.org/10.1002/nag.1610070404.

Peck, R.B., 1969. Advantages and limitations of the observational method in applied soil mechanics. Géotechnique 19, 171–187. http://dx.doi.org/10.1680/geot.1969.19.2.171.

PLAXIS Material Model, 2021. PLAXIS 2D Connect Edition V21 - Material Models Manual. Bentley Systems.

PSCG, 2000. Specifcation for Excavation in Shanghai Metro Construction. Technical Report, Professional Standards Compilation Group, Shanghai, China.

Quang, N.D., Chai, J.C., 2015. Permeability of lime- and cement-treated clayey soils. Can. Geotech. J. 52, 1221–1227. http://dx.doi.org/10.1139/CGJ-2014-0134.

Randolph, M.F., Carter, J.P., Wroth, C.P., 2015. Driven piles in clay—the effects of installation and subsequent consolidation 29. pp. 361–393. http://dx.doi.org/10.1680/GEOT.1979.29.4.361, URL: https://www.icevirtuallibrary.com/doi/10.1680/geot.1979.29.4.361.

Rankka, K., Andersson-Sköld, Y., Hultén, C., Larsson, R., Leroux, V., Dahlin, T., 2004. Quick Clay in Sweden. Technical Report, Swedish Geotechnical Institute, Retrieved from Statens geotekniska institut website: http://urn.kb.se/resolve?urn=urn:nbn:se:swedgeo:diva-220.

Sanlon, P., Sivakumar, V., Solan, B., Tripathy, S., MacKinnon, P., Donohue, S., Ramaiah, B.J., 2021. Assessment of skempton's pore water pressure parameters b and a using a high-capacity tensiometer. Géotechnique 71, 110–119. http://dx.doi.org/10.1680/jgeot.18.P.191.

Schanz, T., 1998. Zur modellierung des mechanischen verhaltens von reibungsmaterialen, habilitation. Stuttgart Universität, Stuttgart, Germany.

Schanz, T., Vermeer, P.A., Bonnier, P.G., 1999. The hardening soil model: Formulation and verification. In: Beyond 2000 in Computational Geotechnics. Ten Years of PLAXIS International. Proceedings of the International Symposium. Amsterdam, March 1999, pp. 281–296. http://dx.doi.org/10.1201/9781315138206-27.

Shen, S.L., Huang, X.C., Du, S.J., Han, J., 2003a. Laboratory studies on property changes in surrounding clays due to installation of deep mixing columns. Mar. Georesour. Geotechnol. 21, 15–35. http://dx.doi.org/10.1080/10641190306711.

Shen, S.L., Miura, N., Koga, H., 2003b. Interaction mechanism between deep mixing column and surrounding clay during installation. Can. Geotech. J. 40, 293–307. http://dx.doi.org/10.1139/t02-109.

Sivasithamparam, N., Karstunen, M., Bonnier, P., 2015. Modelling creep behaviour of anisotropic soft soils. Comput. Geotech. 69, 46–57. http://dx.doi.org/10.1016/J.COMPGEO.2015.04.015.

Sivasithamparam, N., Karstunen, M., Brinkgreve, R.B., Bonnier, P.G., 2013. Comparison of two anisotropic creep models at element level. In: Installation Effects in Geotechnical Engineering - Proceedings of the International Conference on Installation Effects in Geotechnical Engineering. ICIEGE 2013, pp. 72–78.

Stab, E.S., 2002. Development of Design and Construction Methods to Stabilize Soft Organic Soils: Design Guide for Soft Soil Stabilization. CT97-0351, European Commission, Industrial and Materials Technologies Programme (Rite-EuRam III) Bryssel.

Stevens, R.L., Bayard, E., 1994. Clay mineralogy of agricultural soils (ap horizon) in västergötland, sw sweden. GFF 116, 87–91. http://dx.doi.org/10.1080/11035899409546163.

Stevens, R.L., Rosenbaum, M.S., Hellgren, L.G., 1991. Origins and engineering hazards of swedish glaciomarine and marine clays. Geol. Soc. Lond. Eng. Geol. Spec. Publ. 7, 257–264. http://dx.doi.org/10.1144/GSL.ENG.1991.007.01.24, URL: https://egsp.lyellcollection.org/content/7/1/257.

Swedish Transport Administration, 2018. Fullskaleförsök DDM (Dry Deep Mixing) i passivzon, delprojekt E02 Centralen, Västlänken. Technical Report TRV 2015/74805, Swedish Transport Administration (Trafikverket).

Swedish Transport Administration, 2019. Redogörelse för konstruktionsarbetets förutsättningar och metoder (RKFM)-Temporär geokonstruktion: 4.1, 4.3, 4.4 och 5.3. Technical Report, Swedish Transport Administration (Trafikverket).

Tahershamsi, H., Dijkstra, J., 2022. Using experimental design to assess rate-dependent numerical models. Soils Found. 62, 101244. http://dx.doi.org/10.1016/j.sandf.2022.101244, URL: https://www.sciencedirect.com/science/article/pii/S0038080622001524.

Tanaka, H., 1993. Behavior of braced excavations stabilized by deep mixing method. Soils Found. 33, 105–115. http://dx.doi.org/10.3208/SANDF1972.33.2_105.

Tavenas, F., Jean, P., Leblond, P., Leroueil, S., 1983. The permeability of natural soft clays. part ii: Permeability characteristics. Can. Geotech. J. 20, 645–660. http://dx.doi.org/10.1139/t83-073.

Taylor, H.F., et al., 1997. Cement Chemistry. Volume 2. Thomas Telford London.

Tornborg, J., Karlsson, M., Kullingsjö, A., Karstunen, M., 2021. Modelling the construction and long-term response of göta tunnel. Comput. Geotech. 134, 104027. http://dx.doi.org/10.1016/j.compgeo.2021.104027, URL: https://www.sciencedirect.com/science/article/pii/S0266352X21000306.

Trafikverket, 2014. Trafikverkets tekniska krav för geokonstruktioner, TK Geo 13 - ver 1.0.

Vermeer, P., Brinkgreve, R., 1998. Plaxis Finite Element Code for Soil and Rock Analysis. Balkema, Rotterdam-Brookfield, Netherlands, pp. 1–114.

Vogler, U., 2009. Numerical Modelling of Deep Mixing with Volume Averaging Technique (Ph.D. thesis). The University of Strathclyde, URL: https://ethos.bl.uk/OrderDetails.do?uin=uk.bl.ethos.501779.

Wang, D., Tanttu, L.K., 2018. 1-D compressibility behaviour of cement-lime stabilized soft clays. Eur. J. Environ. Civ. Eng. 24, 1013–1031. http://dx.doi.org/10.1080/19648189.2018.1440633.

Wheeler, S.J., Näätänen, A., Karstunen, M., Lojander, M., 2003. An anisotropic elastoplastic model for soft clays. Can. Geotech. J. 40, 403–418.

Yamadera, A., Nagaraj, T.S., Miura, N., 1998. Prediction of strength development in cement stabilised marine clay. In: Proceeding of the Geotechnical Engineering Conference, Vol. 1. Bangkok, pp. 141–153.

Yang, C., Liu, X., Liu, X., Yang, C., Carter, J.P., 2015. Constitutive modelling of otaniemi soft clay in both natural and reconstituted states. Comput. Geotech. 70, 83–95. http://dx.doi.org/10.1016/J.COMPGEO.2015.07.018.

Yapage, N.N.S., Liyanapathirana, D.S., 2019. A review of constitutive models for cement-treated clay. Int. J. Geotech. Eng. 13, 525–537. http://dx.doi.org/10.1080/19386362.2017.1370878.

Yin, J.H., Graham, J., 2011. Equivalent times and one-dimensional elastic viscoplastic modelling of time-dependent stress–strain behaviour of clays 31. pp. 42–52. http://dx.doi.org/10.1139/T94-005, URL: https://cdnsciencepub.com/doi/10.1139/t94-005.

Yin, Z.Y., Karstunen, M., Chang, C.S., Koskinen, M., Lojander, M., 2011. Modeling time-dependent behavior of soft sensitive clay. J. Geotech. Geoenviron. Eng. 137, 1103–1113. http://dx.doi.org/10.1061/(ASCE)GT.1943-5606.0000527.

Zöhrer, W., Stelte, M., 2010. Is ground engineering environmentally friendly? Ecological balance of foundation engineering methods. In: 11th International EFFC-DFI Conference, Session 3: Sustainability in the Foundation Industry.